Weather Types and Rainfall over Senegal. Part I: Observational Analysis

Vincent Moron[1] , Andrew W. Robertson, M. Neil Ward, Ousmane N'Diaye

International Research Institute for Climate and Society,

The Earth Institute at Columbia University

Palisades, New York

submitted to *Journal of Climate*

June, 27 2006

[1] Corresponding author address : Vincent Moron, IRI-Monell 219, 61 Route 9W, Palisades, NY 10964. (email : vincent@iri.columbia.edu). Permanent position : UFR des Sciences Geographiques et de l'Amenagement, Universite d'Aix-Marseille I, and CEREGE, UMR-6635 CNRS

Abstract

A *k*-means cluster analysis is used to summarize unfiltered daily atmospheric variability at regional-scale over the western Sahel and eastern tropical North Atlantic during the boreal summer season (July—September) 1961—1998. It employs zonal and meridional regional wind fields at 925, 700 and 200 hPa from the European Centre for Medium Weather Forecast Reanalyses (ERA-40). An 8-cluster solution is shown to yield an integrated view of the complex regional circulation variability, without the need for explicit time filtering. Five of the weather types identified characterize typical phases of African easterly waves persistent monsoon surges, while the three others describe different stages of the seasonal cycle. Their temporal sequencing describes a systematic monsoonal evolution, together with considerable variability at sub-seasonal and inter-annual time scales.

Daily rainfall occurrence at 13 gauge stations in Senegal is found to be moderately well-conditioned by the 8 weather types, with positive rainfall anomalies usually associated with low-level southerly wind anomalies. Interannual variability of daily rainfall frequency is shown to depend substantially on the frequency of occurrence of weather types specific to the beginning and end of the rainy season, together with the number persistent monsoon surges over the western Sahel. In contrast, year-to-year changes in the frequency of the weather types associated with African Easterly Waves are not found to influence seasonal rainfall substantially.

The fraction of seasonal rainfall variability related to weather type frequency is found to have a strong relationship with tropical Pacific sea surface temperatures: an El Niño (La Niña) event tends to be associated higher (lower) frequency of dry early and late season weather types with

enhanced trade winds over the western Sahel, together with lower (higher) prevalence of persistent monsoon surges. The fraction of seasonal rainfall variability *not* related to weather-type frequency is characterized by changes in rainfall probability within each weather type, especially those occurring in the core of the rainy season, and exhibits a strong decadal component.

1. Introduction

Many previous studies have investigated the inter-annual variability of seasonal mean rainfall in the Sahel region in general (i.e. Nicholson, 1979; Fontaine and Bigot, 1993; Moron, 1994; Rowell *et al.*, 1995; Ward, 1998) as well as for Senegal (Camberlin and Diop, 1999). Folland *et al.* (1986) demonstrated the association between the changes in sea surface temperatures (SST) and Sahelian seasonal mean rainfall variability. They identified a strong relationship between the inter-hemispheric gradient of SST and multi-decadal variability of Sahelian rainfall (Lamb, 1978; Hastenrath, 1984, 1990; Rowell *et al.*, 1995; Ward, 1998). The relationships between SST and Sahelian rainfall at inter-annual time scales are more complex and less stable (Janicot *et al.*, 1996; Ward, 1998). Wetter (drier) conditions in the Sahel are usually associated with cold (warm) El Niño Southern Oscillation (ENSO) events, anomalously cold (warm) SST anomalies (SSTA) over the equatorial and southern Atlantic and the western Indian ocean and anomalously warm (cold) SSTA over the northern tropical Atlantic. These empirical relationships have since been largely confirmed by atmospheric General Circulation Models (AGCM) experiments with historical SST prescribed (Rowell *et al.*, 1995; Moron *et al.*, 1998; Giannini *et al.*, 2003; Paeth and Friederichs, 2004). Such experiments have been highly successful at simulating the multi-decadal variability of Sahelian rainfall (Giannini *et al.,* 2003), but their skill is uneven at inter-annual time scales, especially during the post-1967 dry period (Sperber and Palmer, 1996; Moron *et al.*, 2003; Moron, 2005).

The above studies have focused almost exclusively on seasonal mean rainfall, while very little attention has been given to the inter-annual variability of sub-seasonal quantities such as the number of rainy days, length of dry/wet spells etc. Rainfall over West Africa during the summer

monsoon is mainly associated with meso-scale convective systems (D'Amato and Lebel, 1998; Laurent *et al.*, 1998; Lebel et al., 2003). These are often, but not always, embedded within African easterly waves (Burpee, 1972) that arise from barotropic/baroclinic instability of the middle troposphere African Easterly jet (AEJ) that extends W-E over most of the Sahel near 15°N. Nevertheless, the link between convection (and rainfall) and easterly waves is far from linear and remains controversial (Thorncroft and Rowell, 1998; Diedhiou *et al.,* 1998, 1999, 2001; Grist, 2002; Gu and Adler, 2004; Gu *et al.*, 2004). Fink and Reiner (2003) argue that the strength of coupling between easterly waves and meso-scale convective systems increases toward the West-African coast, consistent with the westward observed growth of wave amplitude. Easterly waves are not the only sub-seasonal modulator of the rainfall. Janicot and Sultan (2001) identified a westward propagating quasi-periodic signal with a period of about 15-40 days associated with the meridional shift of the ITCZ (Sultan and Janicot, 2000) and the surges of the West-African monsoon (Louvet *et al.*, 2003). Even slower sub-seasonal components have also been identified (Sultan *et al.*, 2003; Mathews 2004). In summary, the sub-seasonal variability of rainfall in Sahel is composed of the interactions between inter-related processes with various time and space scales (Sultan *et al.*, 2003). It is little understood how these sub-seasonal processes are influenced by SST forcing.

Most of the studies cited above used band-pass filtered time series to analyze sub-seasonal variability and its relationship with local-to-regional rainfall within a specified frequency range. A different approach is pursued here, based on an objective clustering method (*k*-means) that is used to partition *unfiltered* daily atmospheric variability into different weather types. In the extra-tropics, such a clustering scheme is commonly used to define so-called "weather regimes"

(Mo and Ghil, 1988; Molteni *et al.*, 1990). These weather regimes are usually interpreted as preferred states of a nonlinear dynamical system with a chaotic attractor (Ghil and Robertson, 2002). They are characterized by persistent large-scale flow patterns that appear repeatedly at fixed geographical locations and organize the behavior of synoptic-scale motions during several days or weeks (Michelangeli *et al.*, 1995; Robertson and Ghil, 1999). As the name implies, weather regimes affect local weather. The goals of the present study are; (i) to propose an objective partitioning of the regional-scale atmospheric circulation variability over the western Sahel and eastern Tropical North Atlantic (0-30W, 5-25N), considering all time scales; and (ii) to analyze how these "weather types" affect local rainfall in Senegal. The use of these weather types in downscaling studies is illustrated in part II of this study (Moron *et al.*, 2006b, referred hereafter as Part II).

Section 2 describes the daily station rainfall dataset together with the reanalysis atmospheric circulation data. The weather types are presented in section 3. A summary and conclusions are presented in section 4.

2. Datasets

a. Rainfall

The study uses a 13-station network (Fig. 1c) of daily rainfall observations over Senegal as in Moron *et al.* (2006a). This network includes the 10 main synoptic stations of the country and 3 non-synoptic stations (i.e. Diouloulou, Kounghel and Goudiry). The data used in this study covers the period from July, 1, 1961 to September 30, 1998. Senegal is a flat Sahelian country neighboring the Tropical North Atlantic. As for the entire Sahel, the rainy season grows longer

southward (Fig. 1a,b), associated with the latitudinal migration of the Inter-Tropical Convergence Zone (ITCZ). Daily rainfall occurrence frequency (day receiving > 1 mm) usually peaks between August 25 and September 5, north of 13.5°N (Fig. 1a). The seasonal cycle is flatter for the 4 southernmost stations (i.e. Ziguinchor, Diouloulou, Kolda and Kedougou) with almost no difference between July 20 and September 10 (Fig. 1a). The amplitude of the seasonal cycle is small for the mean daily rain amount on wet days with a peak around the end of August in the northern two-thirds of the country (Fig. 1b); it is also small in southern Senegal (i.e. higher rainfall amount from July 20 to September 10) associated with higher rainfall rates than in the north-central part of the country (Fig. 1b).

b. ERA-40

The ECMWF (European Centre for Medium Range Weather Forecast) 40-year reanalysis project (ERA-40, Simmons and Gibson, 2000) data are used to describe variability of atmospheric circulation. The data are available on a 2.5 x 2.5 grid every 6 hours from September 1, 1957. The daily mean of the zonal and meridional component of the winds at 925, 700 and 200 hPa over the area (30°W-0°, 5°-25°N) from July 1, 1961 to September 30, 1998 are used in the following. Fig. 2 displays the mean July-September climatology of the wind at 925 hPa (Fig. 2c), 700 hPa (Fig. 2b) and 200 hPa (Fig. 2a) and also the seasonal cycle of these winds over Senegal (Fig. 2d,e,f). The low-level winds exhibit the classical low level monsoon flow with a convergence near 7°N over the Tropical Atlantic and shifted northward to near 20°N at 0°E, associated with the thermal low centered over the Sahara (Fig. 2c). The southwesterly flow over Senegal is strongest during late July and is replaced by northeasterlies in September (Fig. 2f). The main feature of the middle troposphere is the African Easterly jet (AEJ) with axis near 15°N (Fig. 2b); it is only weakly

modulated by the seasonal cycle during the period in ERA-40, with a slight weakening after mid-July (Fig. 2e). The Tropical Easterly jet (TEJ) dominates the upper troposphere, with Senegal near its northern margin (Fig. 2a). Its main axis is shifted southward relatively to the AEJ, and its seasonal cycle matches that at lower levels peaking around the end of July (Fig. 2d), i.e. before the peak of the rainy season (Fig. 1a,b). The mean upper-level winds become weak westerlies in late September (Fig. 2d). Note that the ERA-40 fields were firstly linearly interpolated from the original 2.5 x 2.5 degree grid onto a T42 Gaussian grid, to facilitate the analysis in Part II where the ECHAM4.5 GCM simulations are introduced.

3. Weather types

a. Definition of the number of weather types

A standard *k*-means cluster analysis is applied to the 7 leading unstandardized principal components (PC) accounting for 52% of the variance of the ERA-40 daily winds. Considering more PCs, explaining a larger fraction of the variance, yields very similar weather types but slows the computations used in Part II. *K*-means is an iterative clustering procedure (Diday and Simon, 1976) that consists in partitioning the data into *k* clusters so as to minimize the sum of within-cluster variance. The first step concerns choosing the appropriate number of clusters. Because *k*-means minimizes the sum of squared Euclidean distances within the set of clusters, the pseudo-F test could be used. Another possibility is the "red-noise" test used by Michelangeli *et al.* (1995) to select the most robust classification relative to a set of random simulations. However, in this study we are particularly interested in the clusters that discriminate local rainfall over Senegal, suggesting the information criterion defined by Santos *et al.* (2005)

$$I = \sum_{i=1}^{k} \left| n_{i,r} - (p_r \times n_i) \right|. \quad (1)$$

Here $n_{i,r}$ is the number of days in cluster *i* that receive a rainfall amount greater than *r*, p_r is the probability of such rainy days in the whole population, n_i is the number of days in cluster *i* and *k* is the total number of clusters. Fig. 3 shows *I* as a function of *k* for each station, together with the country average. The information criterion *I* exhibits a large jump from 2 to 3 clusters, and a second smaller increase from 6 to 8 clusters. The curve is then almost flat from 8 to 20 clusters. We choose 8 clusters as a compromise between adequate discrimination of local rainfall and physical interpretation of the atmospheric circulation patterns.

b. Temporal sequence of weather types

The chronological sequence of the 8 weather types (WT hereafter) is plotted in Fig. 4. It reveals a spectrum of different time-scales: the occurrence frequency of each WT varies on inter-annual time scales but also within each season. The mean seasonal cycle of each WT, the probabilities of transitions between them, and the spell-length distributions are illustrated in Fig. 5. The occurrence of WT 1, and especially that of WT 7-8, is strongly modulated by the seasonal cycle: WT 1 is prevalent before about July 15, and WT 7-8 after about September 15. WT 1 also occurs also during the core of the rainy season in persistent spells (e.g. 1968, 1972, 1977, 1978, 1981, 1986, and 1987). The WTs 3-6 are most prevalent from about July 10 to about September 20 but rarely persist for more than 5 days, except perhaps for WT 2 (e.g. July 1975, July 1981, and August 1994). The transitions amongst the 5 WTs reveal preferred circuits: 2 → 3 → 4 → 2, and 3 → 4 → 6 → 5 → 3, and 2 → 5 → 3 → 4 → 2 (Fig. 5b), suggesting that these WTs may be associated with easterly waves.

c. Atmospheric patterns

Composite maps of daily wind anomalies for the 8 weather types at 925, 700 hPa are presented in Figs. 6-9. The wind anomalies at 200 hPa are not shown since they mostly reflect the peak of seasonal cycle of each cluster. These figures are organized following the mean seasonal evolution, with the early-season WT 1 shown in Fig. 6, the WTs of the core rainy season displayed together in Figs 7-8 and the late-season WTs 7 and 8 shown in Fig. 9. The composites are plotted as standardized anomalies relative to the long-term July-September mean. Note that the maps of Fig. 6-9 cover a larger area than the window used in the clustering.

With respect to the July-September mean, WT 1 is characterized by an anomalous anticyclone at 700hPa, centered to the west of Senegal (Fig. 6a), with strong surface northerly anomalies to the north, related to anomalous cyclonic centered near 5W-20N (Fig. 6b). These features largely reflect mean conditions during early July when WT 1 is prevalent, prior to the core monsoon season. However, similar composites result if the season is split into two, to consider the early (pre-July 16) and core parts of the season separately (not shown). Thus, WT may be associated with "breaks" during the core monsoon season, with circulation features of early July.

Weather types 2-6 (Fig. 7-8) all exhibit wavy patterns at 925 hPa whose spatial structures are broadly consistent with an easterly wave, then ordered according to the temporal sequences identified in Fig. 5 (Burpee, 1972; Dhiedou *et al.*, 1998, 1999; Grist, 2002). WT 3 is almost a mirror image of WT 6 over the region used to define the clusters (Fig. 7b,e). The patterns of WT 2 and WT 4 are also consistent with slower intra-seasonal modes, such as monsoon surges (Janicot and Sultan, 2001; Sultan *et al.*, 2003) over the western and central Sahel respectively. This is especially true for WT 2, which leads to long persistent spells (Fig. 4 and 5c). The wavy

pattern is also seen at 700 hPa (Fig. 8), with a phase shift consistent with a baroclinic vertical structure (Dhiedou *et al.*, 1998, 1999); the cyclonic anomaly centers at 700 hPa are ~5 deg east-southeast of those at 925 hPa (Fig. 8). These centers are located near 15-17°N (slightly southward for WT 6), which is near the core of AEJ (Fig. 2b). WT 2 has a broader spatial scale, and is characterized by a strong meridional shear about the main axis of the AEJ, known to favor the development of squall lines (Fink and Reiner, 2004). At 200 hPa (not shown), WTs 2-4 are characterized by a broad-scale strengthening of the TEJ near its seasonal peak. At 200hPa, WTs 5-6 are characterized by weak anomalies over the western Sahel, with some evidence of wave patterns near 30N (not shown).

Composites for the late-season WTs are shown in Fig. 9 over a broader region to highlight possible connections with the midlatitude circulation in the transition season. They are characterized by a simple pattern at 200 hPa (not shown), with a broad-scale westerly anomaly associated with the disappearance of the TEJ at the end of the rainy season (Fig. 2e). A trough in the subtropical westerly jet near the African coast is observed in WT 8, while a slight anomalous ridging there is visible in WT 7. These westerly anomalies are vertically extensive, also visible at 700 hPa, though with large differences between states 7 and 8 over Senegal (Fig. 9a,b). A strengthening and/or southward shift of the AEJ at 700hPa is visible near 9N in both WTs (Fig. 9a,b). At 925hPa, an anomalous anticyclonic center characterizes both WTs 7 and 8, with anomalous northeasterlies over western and central Sahel (Fig. 9c,d)..

d. Relationship between the weather states and rainfall occurrence

A central objective of this study is to relate the above circulation regimes to rainfall over Senegal. Figure 10 shows the spatial distribution of daily rainfall occurrence as anomalies relative to the long-term mean. Weather types 1, 4 and 7 are the driest, and WTs 2, 5 and 6 the wettest. This basic differentiation is partly related to their seasonality since the seasonal cycle of rainfall (Fig. 1a,b) has been retained in the rainfall time series. However, WT 1 is clearly identified with dry spells during the core of the rainy season as well (Figs. 4,5). The easterly-wave WT sequences depicted in Figs. 7-8 are indeed consistent with a westward propagating rain event. Positive rainfall anomalies in WT 2, 5 and 6 coincide with (or just east in case of WT 5) the S-SW wind anomalies at 925 hPa (Fig. 7a,c,e) while negative rainfall anomalies in WTs 3 and 4 are located within the NW anomalies at 925 hPa (Fig. 7b,d). Weather types 7 and 8 are anomalously dry with respect to the seasonal average, consistent with their seasonality. However, WT 8 is anomalously wet with respect to the late-September average.

f. Interannual variability of weather types and seasonal rainfall in Senegal

The connection between weather type and rainfall occurrence over Senegal suggest that it may be possible to use the weather types as a tool to interpret seasonal-scale rainfall anomalies in terms of year-to-year anomalies in weather-type frequency. In the following, "seasonal rainfall" will refer to seasonal rainfall occurrence frequency. Considering seasonal rainfall amounts instead of rainfall occurrence leads to similar results (not shown), but with slightly weaker relationships for amounts. This is consistent with the slightly higher spatial coherence and potential predictability of rainfall frequency compared to seasonal amount (Moron *et al.*, 2006a).

Figure 11 shows the relationship between the frequency occurrence of each WT and seasonal rainfall, for the 10 driest and wettest years, in terms of the standardized anomaly index *SAI* of rainfall occurrence. The SAI is defined as the station-average of the standardized anomalies at each station. For the "seasonal" WTs 1, 2 and 8, the differences in WT frequency between the two sets of years are consistent the mean rainfall anomaly of each WT. Thus the 10 driest years contain more of WT 1 and 8, but less of WT 2 (Fig. 11a-b,h).

Differences in frequency of WT 4-7 are not significant overall between the wet and dry years, although shifts in WT seasonality can be identified (Fig. 11d-g). There are slightly more WT 6 (wet) in dry years (Fig. 11f), but this increased prevalence is concentrated in September, when rainfall is climatologically small (Fig. 1a). The relationship between WT 3 and seasonal rainfall is complex. On average, this WT is accompanied by weakly negative rainfall anomalies (Fig. 10c), yet there are clearly more WT 3 days in wet years than in dry years (Fig. 11c). This can be explained by differences in transition probabilities into WT 3 between the two sets of years, with more-frequent transitions from state 5 in dry years. WT 3 days exhibit 10-40% higher rainfall probabilities when they follow WT 2 as opposed to WT 5.

g. Canonical correlation analysis

Clearly, year-to-year changes in WT frequency cannot account for all interannual variability of rainfall. Even if the frequency of a WT remains constant, it may be associated with wetter conditions in some years than others. In this sub-section we estimate the relative importance of changes in WT frequency vs. changes in WT "character" (i.e. its rainfall characteristics), for interannual rainfall variability over Senegal. As in the preceding section, we confine our

attention to rainfall occurrence only. Similar results are obtained using amounts, with a slight decrease of skill.

The number of wet days $N_{i,j}$ in year i at station j can be decomposed into the rainfall probability for each weather type $p_{i,j,k}$ in year i at station j, multiplied by the frequency of each weather type $n_{i,k}$ during that year

(2) $$N_{i,j} = \sum_{k=1}^{8} p_{i,j,k} n_{i,k}$$

Two complementary Canonical Correlation Analyses (CCA, Barnett and Preisendorfer, 1987; Ward and Navarra, 1997; Moron et al., 2001) are made to estimate the contribution of $n_{i,k}$ (i.e. WT frequency) and $p_{i,j,k}$ (i.e. WT character) in explaining $N_{i,j}$. The first CCA is made between $n_{i,k}$ and $N_{i,j}$, so that WT frequency is used to "predict" rainfall variability. The second CCA uses $p_{i,j,k}$ as the predictor. Both CCAs are applied using cross-validation, leaving out 5 consecutive years each time, and computing the CCA on the remaining 33 years. We restrict our attention to the leading CCA mode in each case, since inclusion of subsequent modes is not found to significantly increase the skill.

Results of the first CCA between $n_{i,k}$ and $N_{i,j}$ are presented in Fig. 12, in terms of correlation between the "predicted" and observed rainfall occurrence frequency $N_{i,j}$ at each station (panel a), the loading of each WT's frequency $n_{i,k}$ (panel b), and the cross-validated CCA time scores (panel c). The skill of WT frequency is spatially homogenous, with value between 0.36 and 0.60, except at Kedougou in the extreme SE of the country (Fig. 12a). More than 50% of the

station variance is explained by this mode at 8 out of the 13 stations. The WT loadings are characterized by large positive loadings for WT 2 and 3, and strong negative loadings for WT 1 and 8 (Fig. 12b). Thus, changes in WT frequency during the onset and end phases of the monsoon (WT 1 and 8), breaks in the monsoon (WT 1), and surges during the core of the rainy season (WT 2) exert the largest impact on the interannual variability of rainfall occurrence. On the other hand, changes in the frequency of the WTs, interpreted mainly as phases of easterly waves, are not significant in explaining the interannual variability of rainfall (Fig. 12b)

The temporal scores (Fig. 12c) suggest that the intensity of the link between WT frequency and rainfall occurrence has weakened since 1980. The correlation between both CCA time series is 0.60 for the whole period but drops from 0.81 in 1961-1979 to only 0.36 in 1980-1998.

The complementary CCA between $N_{i,j}$ and the year-to-year changes in the probability of rainfall in each weather type $p_{i,j,k}$, is presented in Fig. 13. The skill values, using $p_{i,j,k}$ as the predictor (panel a) are somewhat higher than those in Fig. 12a, especially in the central-northern part of Senegal. In this case, the loadings of each WT (panel b) are consistently positive with largest values for WTs whose frequency peaks in the core of the rainy season. The correlation between cross-validated CCA temporal scores is 0.80 (panel c) with similar values for the first and second halves of the time series (0.79 and 0.81 respectively).

The predictions of station-average SAI of rainfall occurrence made with the two CCA analyses are plotted in Fig. 14, together with the observed SAI. The two predictions are seen to be quite independent (r = 0.28). During certain years, such as the 1972 dry year, the contribution of WT

frequency is particularly large, mostly associated with an abundance of "dry" WT 1 (41 days) and no wet WT 2 (Fig. 4). However, the discrepancy between observed SAI and its prediction from WT-frequency is large in 1965, 1980, 1982, 1987, 1991 and 1992, where year-to-year changes in $p_{i,j,k}$ are clearly important. The low-frequency component of the CCA predictions is plotted in Fig. 14b. Clearly changes in WT-character $p_{i,j,k}$ are most important in accounting for decadal variability of rainfall frequency over the Sahel.

h. Relationships with sea surface temperature

To gain further insight, we plot correlations between the CCA modes and SST in Fig. 15. Correlations with the observed *SAI* (panel a) show the well-known SSTA structure familiar from previous analyses of Sahelian rainfall (i.e. Fontaine and Bigot, 1993; Rowell *et al.*, 1995; Ward, 1998; Janicot *et al.*, 2001). Positive rainfall anomalies are associated with La Niña-like SST anomalies over the tropical Pacific, cold SSTAs over the Indian Ocean and warm SSTAs over the tropical North Atlantic. As noted by Rowell (2001), the highest correlations in tropical Pacific are shifted south of the equator relative to the canonical ENSO SST pattern (Rasmusson and Carpenter, 1982). The fact that correlations are weak over the Atlantic could be associated with the relatively short period of the analysis. This would tend to underemphasize the multi-decadal variability, which is strongly correlated with Atlantic SSTAs (Folland *et al.*, 1986; Rowell *et al.*, 1995).

The SST correlations with the leading CCA mode of WT frequency (Fig. 15b) are very clearly dominated by ENSO. The correlations over the Tropical Pacific are now almost symmetric relative to the equator and match the canonical ENSO pattern (Rasmusson and Carpenter, 1982).

In contrast, the SST correlations with the complementary leading CCA mode of WT character (Fig. 15c) are generally weak, tending to resemble the other aspects of the correlations with the SAI over the Atlantic, west Pacific and Indian Oceans. Over the tropical Pacific, the equatorial correlations are close to zero, and the highest values clearly shifted south of the equator (Fig. 15c).

The analysis of SST correlations provides further evidence that the influence of ENSO on Senegal rainfall is largely through changes in WT frequency, while the character of the WTs themselves undergoes important modulation at decadal time scales.

4. Summary and discussion

a. Summary

An objective classification procedure using the *k*-means algorithm was used to summarize the daily atmospheric variability during the boreal summer season 1961-1998 over the western Sahel and eastern Tropical North Atlantic (0-30W, 5-25N). The clustering scheme was based on regional gridded wind fields from the daily ERA-40 reanalyses of the monsoon flow at 925 hPa, the African Easterly Jet level at 700 hPa and the Tropical Easterly Jet level at 200 hPa. An 8-cluster solution was shown to offer a good balance between the discrimination of daily rainfall (Fig. 10) and physical interpretation of the associated atmospheric circulation patterns (Figs. 6-9)

Three of the weather types were found to correspond primarily to the onset (WT 1, Fig. 6) and end of the monsoon season (WTs 7-8, Fig. 9). Weather type 1 was also found to be associated with dry spells during the core of the rainy season WT 1 (Fig. 5). WT 8 may be associated with

late-season interactions with the extratropics (Fig. 9), leading to scattered rainfall mainly over NW Senegal.

Weather types 2-6 were found to be associated with easterly waves and monsoon surges (Fig. 7-8). They are most prevalent from mid-July to mid-September (Fig. 5a) and are generally less persistent than WT 1, 7 and 8, with the exception of WT 2 (Fig. 5c). Two main circuits of transition between these types were identified, with $2 \rightarrow 3 \rightarrow 4 \rightarrow 2$ predominant during the first part of the rainy season, and $3 \rightarrow 4 \rightarrow 6 \rightarrow 5 \rightarrow 3$ during the second part (Fig. 5b). Both circuits are consistent with a westward-moving easterly waves (period 3-9 days and wavelength 2000-3000 km). WT 2 exhibits longer spells of 3-7 days (Fig. 5c) and a pattern characteristic of the monsoon surge over western Sahel (Fig. 7a).

Weather types 2, 5 and 6 were found to be characterized by anomalously high rainfall occurrence over Senegal (Fig. 11b,e,f) with WT 3, and particularly WT 4, being anomalously dry (Fig. 11c,d). However, these relationships with rainfall are not unique. For example, WT 3 tends to be anomalously dry when it follows WT 5, but anomalously wet when it follows WT 2. The more frequent $5 \rightarrow 3$ transition leads to a weak negative mean rainfall anomaly associated with WT 3 (Fig. 11c).

Canonical correlation analysis was used to quantify the extent to which the interannual variability of rainfall occurrence is related to the occurrence-frequency of weather types versus year-to-year changes in the character of the weather types. The frequency of early and late-season weather types (WT 1, 7-8), as well as the frequency of the long-lasting spells of WT 2,

were found to be strongly related to seasonal rainfall, particularly in central and northern Senegal. By contrast, the frequencies of easterly-wave WTs 4-6, were not found to have a significant impact on interannual rainfall variability (Figs. 12-13), consistent with previous findings (i.e. Rowell, 2001: Fink and Reiner, 2002; Fink *et al.* 2004, 2006).

The component of seasonal rainfall associated with changes in WT frequency was found to be strongly related to ENSO (Fig. 15b). El Niño events tend to be associated with more (less) WT 1, 7 and 8 (WT 2-3) and vice-versa for La Niña events. The complementary component not explained by weather-type frequency is characterized by a consistent increase/decrease of probability of rainfall for each WT, especially those that occur during the core of the rainy season (Fig. 15c). This signal explains a larger part of the interannual variance of the country-averaged rainfall occurrence. It was found to less related to ENSO, and to have a stronger decadal component.

b. Discussion

Our findings demonstrate that weather typing using cluster analysis of daily circulation fields over the western Sahel and neighboring Tropical Northern Atlantic is able to recover the main features of circulation variability, without the need to resort to explicit time filtering of the data, as is commonly done. The resulting description gives an integrated view of the complex regional-scale atmospheric circulation features on a mix of different spatial (e.g. meridional migration of the ITCZ, easterly waves, persistent monsoon surges and breaks, tropical-extratropical interactions) and temporal (e.g. seasonal cycle, sub-seasonal variability etc.) scales, leading to rainfall variability from Senegal to Morocco (Knippertz, 2003; Knippertz *et al.*, 2005).

Weather type 1, is of particular interest in this respect, being associated with both the pre-monsoonal seasonal dryness in early July, as well as monsoon breaks during the core monsoon season.

The discrimination of station rainfall frequency by the weather types is significant, but it will be of interest to compare the benefits of this approach with a state classification based directly on the station rainfall observations themselves, such as with hidden Markov models. A match between weather-typing and HMM state classifications would only be expected if local-scale rainfall is uniquely conditioned by the larger scale atmospheric circulation. On the other hand, two similar regional-scale patterns may not necessarily be associated with the same station rainfall pattern and vice-versa. The degree of complexity may vary significantly across the Tropics, depending on the rainfall-generating phenomena. The performance of weather typing and HMM approaches to downscaling from a GCM is explored in part II of this study.

A potentially important result provided by the weather typing is the separation of interannual rainfall variance into a component that is associated with year-to-year changes in weather-type frequency, and a component that is not. The component of rainfall associated with weather-type frequency largely accounts for the relationship with between Senegal rainfall and ENSO. The weather types more prevalent during warm ENSO events are all associated with enhanced north-easterlies at low levels over the western Sahel and/or the neighboring Tropical North Atlantic, consistent with previous findings at the seasonal time scale (i.e. Trzaska *et al.*, 1996; Janicot *et al.*, 1998, 2001; Rowell, 2001). These results are also consistent with previous findings that a late onset and early cessation of rainfall in Senegal often occurs during warm ENSO events but never

during cold events (Camberlin and Diop, 2003, their Fig. 7). Our finding that the frequency of easterly-wave weather types is unrelated to ENSO is consistent with the conclusion of Rowell (2001). The relationship between the weather-type frequency and rainfall variability appears to weaken after 1980, and further work is needed to determine whether this is more than just random sampling variability (Moron *et al.*, 2003; Moron, 2005).

The component of country-averaged rainfall occurrence not associated with weather-type frequency accounts for a larger part of the interannual rainfall variance. It appears to be stronger on longer time scales, and may be the key factor in accounting for trends in Sahelian rainfall. This component could perhaps be associated with a large-scale variation of a circulation-independent process linked to rainfall, such as the availability of moisture, while the ENSO teleconnection is more dynamical. However, the interpretation remains speculative because of the short 1961-98 record of daily station rainfall available.

This study provides a framework for downscaling the local rainfall from atmospheric circulation patterns. If a GCM is able to simulate these weather types sufficiently accurately, together with aspects of their temporal variability, transfer functions could be used to associate these regional-scale patterns with local-scale rainfall. This is explored in Part II of this paper.

Acknowledgments

ECMWF ERA-40 wind data used in this study have been obtained from the ECMWF data server (http://data.ecmwf.int/data/d/era40_daily/). We would like to thank also DMN-Senegal for

providing the daily rainfall dataset for Senegal and Bernard Fontaine, Benjamin Sultan, and Peter Knippertz for their insightful comments at various stages of this study.

References

Barnett T.P., and R. Preisendorfer, 1987: Origins and levels of monthly and seasonal forecast skill for united-states surface air temperatures determined by canonical correlation analysis. *Mon. Wea Rev.*, **115**, 1825-1850.

Burpee R.W., 1972: The origin and structure of easterly waves in the lower troposphere in North Africa. *J. Atmos. Sci,* **29**, 77-90.

Camberlin P., and M. Diop, 1999: Interrelationships between groundnut yield in Senegal, Interannual rainfall variability and sea surface temperatures. *Theor. Appl. Climatol*., **63**, 163-181.

Camberlin P., and M. Diop, 2003: Application of daily rainfall principal component analysis to the assessment of the rainy season characteristics in Senegal. *Climate Research*, **23**, 159-168.

D'Amato N., and T. Lebel, 1998: On the characteristics of the rainfall events in the Sahel with a view to the analysis of the climatic variability. *Int. J. Climatol*., **18**, 955-974.

Diday E., and J.C. Simon, 1976: Clustering analysis. In Digital Pattern recognition, Fu KS (editor) Communication and cybernetics, Vol. 10, Springer-Verlag, 47-94.

Diedhiou A., S. Janicot, A. Viltard, and P. De Felice, 1998: Evidence of two states of easterly waves over West-Africa and Tropical Atlantic, *Geophys. Res. Letters*, **25**, 2805-2808.

Diedhiou A., S. Janicot, A. Viltard, P. De Felice, and H. Laurent, 1999: easterly wave states and associated convection over West-Africa and tropical Atlantic: results from the NCEP/NCAR and ECMWF reanalyses. *Clim. Dyn.*, **15**, 795-822.

Diedhiou A., S. Janicot, A. Viltard, and P. De Felice, 2001: Composite patterns of easterly disturbances over West-Africa and the tropical Atlantic: a climatology from the 1979-1995 NCEP/NCAR reanalyses. *Clim. Dyn.*, **18**, 241-253.

Ebisuzaki W., 1997: A method to estimate the statistical significance of a correlation when the data are serially correlated. *J. Climate*, **10**, 2147-2153.

Fink A.H., and A. Reiner, 2003: Spatio-temporal variability of the relation between African easterly waves and West African Squall lines in 1998 and 1999. *J. Geophys. Res.*, **108**, D114332, doi:10.1029/2002JD002816.

Fink A.H., D.G. Vincent, P. Reiner, and P. Speth, 2004: Mean state and wave disturbances during phase I, II and III of GATE based on ERA-40. *Mon. Wea. Rev.*, **132**, 1661-1683.

Folland C.K., T.N. Palmer, and D.E. Parker, 1986: Sahel rainfall and worldwide sea temperatures. *Nature*, **320**, 602-607.

Fontaine B., and S. Bigot, 1993: West-African rainfall deficits and sea surface temperatures, *Int. J. Climatol.*, **13**, 271-285.

Ghil M., and A.W. Robertson, 2002: "Waves" vs. "particles" in the atmosphere's phase space: A pathway to long-range forecasting. *Proc. Nat. Acad. Sci*, **99**, 2493-2500.

Giannini A., R. Saranavan, and P. Chang, 2003: Oceanic forcing of Sahel rainfall on interannual to interdecadal timescales, *Science*, **302**, 1027-1030.

Grist J.P., 2002: Easterly waves over Africa. Part I: the seasonal cycle and contrasts between wet and dry years. *Mon. Wea. Rev.*, **130**, 197-211.

Gu G., and R.F. Adler, 2004: Seasonal evolution and variability associated with the West-African monsoon system. *J. Climate*, **17**, 3364-3377.

Gu G., R.F Adler, G.J Huffman, and S. Curtis, 2004: African easterly waves and their association with precipitation. *J. Geophys. Res.*, **109**, D04101, doi:10.1029/2003JD003967.

Hastenrath S., 1984: Interannual variability and annual cycle: mechanisms of circulation and climate in the tropical Atlantic. *Mon. Wea. Rev.*, **112**, 1097-1107.

Hastenrath S., 1990: Decadal scale changes of the circulation in the tropical Atlantic sector associated with Sahel drought. *Int. J. Climatol.*, **10**, 459-472.

Janicot S., V.Moron, and B. Fontaine, 1996: Sahel drought and ENSO dynamics. *Geophys. Res. Letters*, **23**, 515-518.

Janicot S., A. Harzallah, B. Fontaine, and V. Moron, 1998: West African monsoon dynamics and eastern equatorial Atlantic and Pacific SST anomalies (1970-1988). *J. Climate*, **11**, 1874-1882.

Janicot S., and B. Sultan, 2001: Intra-seasonal modulation of convection in the West-African monsoon. *Geophys. Res. Letters*, **28**, 523-526.

Janicot S., P. Camberlin and I. Poccard, 2001: Summer Sahel-ENSO teleconnection and decadal time scale SST variations. *Climate Dyn.*, **16**, 272-289.

Knippertz P., 2003: Tropical-extratropical interactions causing precipitation in northwest Africa: Statistical analysis and seasonal variations, *Mon. Wea. Rev.*, **131**, 3069-3076.

Knippertz P., and J.E. Martin, 2005: Tropical plumes and extreme precipitation in subtropical and tropical West Africa, *Quart. J. Meteo. Soc.*, **131**, 2337-2361.

Lamb P.J., 1978: Large-scale tropical Atlantic surface circulation patterns associated with Subsaharan weather anomalies, *Tellus A*, **30**, 240-251.

Laurent H., N. D'Amato, and T. Lebel, 1998: How important is the contribution of the mesoscale convective complexes in the Sahelian rainfall ? *Phys. Chem. Earth*, **23**, 629-633.

Lebel T., A. Diedhiou, and H. Laurent, 2003: Seasonal cycle and interannual variability of the sahelian rainfall at hydrological scales. *J. Geophys. Res.*, 108, doi:10.1029/2001JD001580.

Louvet S., B. Fontaine and P. Roucou, 2003: Active phases and pauses during the installation of the West-African monsoon through 5-day CMAP rainfall (1979-2001). *Geophys. Res. Letters*, **30**, 2271, doi:10.1029/2003GL018058

Matthews A.J., 2004: Intraseasonal variability over Tropical Africa during northern summer. *J. Climate*, **17**, 2427-2440.

Michelangeli P.A., R. Vautard, and B. Legras, 1995: Weather regimes – recurrence and quasi-stationnarity, *J. Atmos. Sci.*, **52**, 1237-1256.

Mo K.T., and M. Ghil, 1988: Cluster analysis of multiple planetary flow regimes, *J. Geophys. Res.*, **93**, 10927-10952.

Molteni F., S. Tibaldi, and T.N. Palmer, 1990: Regimes in the wintertime circulation over Northern extratropics. 1. Observational evidence. *Quart. J. Meteo. Soc.*, **116**, 31-67.

Moron V., 1994: Guinean and sahelian rainfall anomaly indices at annual and monthly time scales (1933-1990), *Int. J. Climatol*., **14**, 325-341.

Moron V., A. Navarra, M.N. Ward, and E. Roeckner, 1998: Skill and reproductibility of seasonal rainfall patterns in the tropics in ECHAM-4 GCM simulations with prescribed SST, *Clim. Dyn.*, **14**, 83-100.

Moron V., A. Navarra, and M.N. Ward, 2001: Observed and SST-forced seasonal rainfall variability across Tropical America. *Int. J. Climatol.*, **21**, 567-601.

Moron V., Philippon N., and B. Fontaine, 2003: Skill of Sahel rainfall variability in four atmospheric GCMs forced by prescribed SST, *Geophys. Res. Letters*, **30**, 2221.

Moron V., 2005: Skill of sahelian rainfall index in two atmospheric general circulation models ensemble forced by prescribed sea surface temperatures. *CLIVAR exchanges*, 33, 14-19.

Moron V., A.W. Robertson, and M.N Ward, 2006a: Seasonal predictability and spatial coherence of rainfall characteristics in the tropical setting of Senegal. *Mon. Wea. Rev.*, in press.

Moron V., A.W. Robertson, M.N. Ward, and O. Ndiaye, 2006b: Weather types and rainfall in Senegal. Part II: Downscaling with local scaling, k nearest neighbor analog, weather classification and hidden Markov models. *J. Climate*, submitted.

Nicholson S.E., 1979: Revised rainfall series for the West-African subtropics, *Mon. Wea. Rev.*, **107**, 620-623.

Paeth H., and P. Friederichs, 2004: Seasonality and time scales in the relationship between global SST and African rainfall, *Clim. Dyn.*, **23**, 815-837.

Rasmusson E.M., and T.H. Carpenter, 1982: Variations in tropical sea-surface temperature and surface wind fields associated with the southern oscillation El-Nino. *Mon. Wea. Rev.*, **110**, 354-384.

Robertson A.W., and M. Ghil, 1999: Large-Scale Weather Regimes and Local Climate Over the Western United States. *J. Climate*, **12**, 1796-1813

Robertson A. W., S. Kirshner, and P. Smyth, 2004: Downscaling of daily rainfall occurrence over Northeast Brazil using a Hidden Markov Model. *J. Climate,* **17**, 4407-4424.

Robertson A. W., S. Kirshner, P. Smyth, S.P. Charles, and B.C. Bates, 2006: Subseasonal-to-Interdecadal Variability of the Australian Monsoon Over North Queensland. *Quart. J. Royal Meteor. Soc.,* **132***,* 519-542.

Rowell D.P., C.K. Folland, K. Maskell, and M.N. Ward, 1995: Variability of summer rainfall over tropical North Africa (1906-1992) : observations and modelling. *Quart. J. Meteo. Soc.*, **113**, 669-704.

Rowell D.P., 2001: Teleconnections between the tropical Pacific and the Sahel. *Quart. J. Meteo. Soc.*, **127**, 1683-1706.

Santos J.A., J. Corte-Real, and S.M. Leite, 2005: Weather regimes and their connection to the winter rainfall in Portugal*, Int. J. Climatol.*, **25**, 33-50.

Simmons A.J., and J.K. Gibson, 2000: The ERA-40 project plan, ERA-40 project report series n 1, ECMWF, Reading, 63 pp.

Sperber K.R. and T.N. Palmer, 1996: Inter-annual tropical rainfall variability in General Circulation Model simulations associated with the Atmospheric Model Intercomparison Project. *J. Climate*, **9**, 2727-2750.

Sultan B., and S. Janicot, 2000: Abrupt shift of the ITCZ over West-Africa and intra-seasonal variability. *Geophys. Res. Letters*, **27**, 3353-3356.

Sultan B., S. Janicot, and A. Diedhiou, 2003: The West-African monsoon dynamics. Part I : documentation of intra-seasonal variability. *J. Climate*, **16**, 3389-3405.

Thorncroft C.D., and D.P. Rowell, 1998: Interannual variability of African wave activity in a general circulation model. *Int. J. Climatol.*, **18**, 1305-1323.

Trzaska S., V. Moron, and B. Fontaine, 1996: Global atmospheric response to specific linear combination of the main SST modes. Part I: numerical experiments and preliminary results. *Ann. Geophysicae*, **14**, 1066-1077.

Vautard R, Mo K.C., and M. Ghil, 1990: Statistical significance test for transition matrices of atmospheric Markov chains. *J. Atmos. Sci.*, **47**, 1926-1931.

Ward M.N., and A. Navarra, 1997: Pattern analysis of SST-forced variability in ensemble GCM simulations: Examples over Europe and the tropical Pacific. *J. Climate*, 10, 2210-2220.

Ward M.N., 1998: Diagnosis and short-lead time prediction of summer rainfall in tropical North Africa at interannual and multidecadal timescales. *J. Climate*, **11**, 3167-3191.

Reference captions

Figure 1: (a) Mean daily rainfall frequency (in % of wet days receiving more than 1 mm of rainfall) at each station and (b) mean daily rainfall amounts (in mm / day in wet days) for the 13 stations of the observed network. The curves represent a smoothed seasonal cycle (low-pass recursive filter retaining only frequencies lower than 1/30 cycle-per-day). The number refers to each station on the location map (c) (1: Podor, 2: St Louis, 3: Linguere, 4: Dakar-Yoff, 5: Diourbel, 6: Kaolack, 7: Goudiry, 8: Kounghel, 9: Tambacounda, 10: Kolda, 11: Kedougou, 12: Diouloulou, 13: Ziguinchor).

Figure 2: Climatological mean of ERA-40 winds in July-September 1961-1998 (a) 925 hPa; (b) 700 hPa and (c) 200 hPa. The right column displays the seasonal cycle (= mean of daily values filtered by a low-pass recursive filter retaining only frequencies lower than 1/30 cycle-per-day) of the (d) 925 hPa, (e) 700 hPa and (f) 200 hPa winds averaged over the 9 grid-points covering Senegal (i.e. 12.5-17.7W and 12.5-17.5N) delineated as a black box on panels (a-c).

Figure 3: Country average of the normalized information criterion computed on daily rainfall (line and circle : rain > 0 mm ; line and square : rain > 1 mm ; line and cross : rain > 2 mm ; line and lower triangle : rain > 5 mm ; line and upper triangle : rain > 10 mm). The 2-20 clusters are defined with k-means on the 7 leading Principal components of zonal and meridional component of ERA-40 winds at 925, 700 and 200 hPa.

Figure 4: Weather type (WT) sequence for each year (WT 1 = black point ; WT 2 = red circle ; WT 3 = red filled square ; WT 4 = red diamond ; WT 5 = blue filled lower triangle ; WT 6 = blue upper triangle ; WT 7 = green cross ; WT 8 = green +).

Figure 5: (a) Seasonal variation of the weather type The seasonal cycle (= mean of daily value) is smoothed by a low-pass filter retaining periods lower than 1/30 cycle-per-day; (b) probability

transition between the weather types The arrows indicate the transition that occurs more likely than chance at the 0.01 level and the circles around the weather types is proportional to the probability; (c) % of days of each types included in homogenous spells of lasting at least 3, 5 and 7 days.

Figure 6: Mean composite of (a) 700 hPa, and (b) 925 hPa anomaly winds of weather type (WT) 1. The raw data from July, 1961 to September 30, 1998 are just normalized to zero mean and unit variance before the computation of the composite. The weather types are computed from wind data in 30W-0; 2.5-27.5N.

Figure 7: Mean composite of 925 hPa anomaly winds for (a) weather type (WT) 2, (b) WT 3, (c) WT 5 (a), WT 4 (e) and WT 6 (f). The arrows indicate the significant transitions between the WTs (see Fig. 5b). The raw data from July, 1961 to September 30, 1998 are just normalized to zero mean and unit variance before the computation of the composite. The weather types are computed from wind data in 30W-0; 2.5-27.5N.

Figure 8: Same as figure 7 for 700 hPa anomaly winds.

Figure 9: Mean composite of (a) 700 hPa for weather type (WT) 7, (b) 700 hPa for WT 8, (c) 925 hPa for WT 7, (d) 925 hPa for WT 8 anomaly winds. The raw data from July, 1961 to September 30, 1998 are just normalized to zero mean and unit variance before the computation of the composite. The weather types are computed from wind data in 30W-0; 2.5-27.5N.

Figure 10: Rainfall occurrence anomalies associated for (a) weather type (WT) 1, (b) WT 2, (c) WT 3, (d) WT 4, (e) WT 5, (f) WT 6, (g) WT 7, (h) WT 8. Significant values at the one-sided 0.01 level according to a chi-square test (null hypothesis is that the probability of rainfall > 1 mm during the days belonging to a given cluster is the same as the one of the remaining days) are shaded.

Figure 11: Seasonal cycle of frequency (a) weather type (WT) 1, (b) WT 2, (c) WT 3, (d) WT 4, (e) WT 5, (f) WT 6, (g) WT 7, (h) WT 8 for the 10 driest (full line) and 10 wettest (dashed line) July-September seasons. The extreme seasons are determined from the standardized anomaly index of rainfall occurrence (= number of wet day > 1 mm) and daily frequency of each WT has been smoothed by a recursive low-pass filter retaining only frequencies lower than 1/30 cycle-per-day. A dot on each curve indicates a significant difference between both samples at the two-sided 0.05 level according to a Student's T test (null hypothesis is that the mean frequency of both samples is equal). The mean occurrence frequency for each WT during the 10 driest and 10 wettest seasons are indicated (in days per July-September season) in the upper right corner of each panel with the significance Student's T test value (null hypothesis is that the mean frequency of both samples is equal).

Figure 12: Homogenous correlations for (a) Observed rainfall occurrence and (b) Weather type frequency of the first mode of a cross-validated CCA between both fields. The homogenous correlations are the correlations between one field and the cross-validated time scores associated with its CCA pattern. (c) cross-validated time series of the first CCA mode (rainfall occurrence in full line + circle and weather type frequency in dashed line + square).

Figure 13: Homogenous correlations for (a) observed rainfall occurrence and (b) Probability of rainfall occurrence of each weather type of the first mode of a cross-validated CCA between both fields. The homogenous correlations are the correlations between one field and the cross-validated time scores associated with its CCA pattern. (c) Cross-validated time series of the first CCA mode (rainfall occurrence in full line + circle and probability of rainfall occurrence in dashed line + square)

Figure 14: (a) Standardized anomaly index (*SAI*) of observed rainfall occurrence (full bold line), estimated rainfall occurrence hindcast by the CCA between rainfall occurrence and probability of rainfall occurrence of each weather type (full line + circle), and by the CCA between rainfall occurrence and weather type frequency (full line + square). (b) Same as (a) for the low-frequency component. The low-frequency is extracted by a recursive low-pass filter removing high frequencies higher than 1/8 cycle-per-year.

Figure 15: Correlation between observed SST in July-September and (a) observed *SAI* (from rainfall occurrence > 1 mm), (b) CCA#1 time score of the weather type frequency and (b) CCA#1 time score of the probability of rainfall of each weather type. The contours are indicated at -0.6, -0.4, -0.2, 0, 0.2, 0.4, 0.6 and shadings indicate local significant correlations at the two-sided 0.05 level according to a random-phase test.

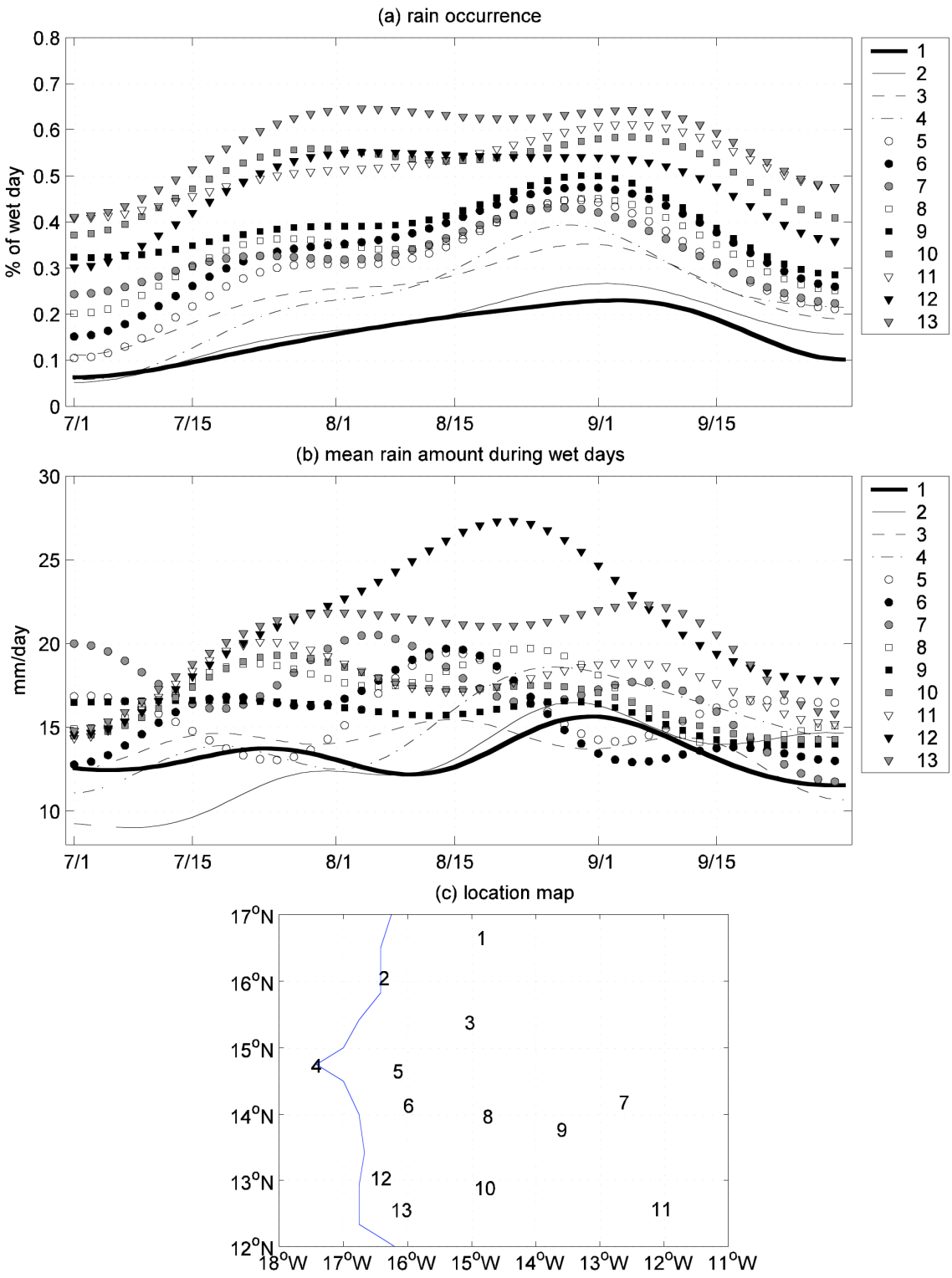
(a) rain occurrence
% of wet day
0.8
0.7
0.6
0.5
0.4
0.3
0.2
0.1
0
7/1
7/15
8/1
8/15
9/1
9/15
1
2
3
4
5
6
7
8
9
10
11
12
13
(b) mean rain amount during wet days
mm/day
30
25
20
15
10
7/1
7/15
8/1
8/15
9/1
9/15
1
2
3
4
5
6
7
8
9
10
11
12
13
(c) location map
17°N
16°N
15°N
14°N
13°N
12°N
18°W
17°W
16°W
15°W
14°W
13°W
12°W
11°W
1
2
3
4
5
6
7
8
9
10
11
12
13

FIG.1

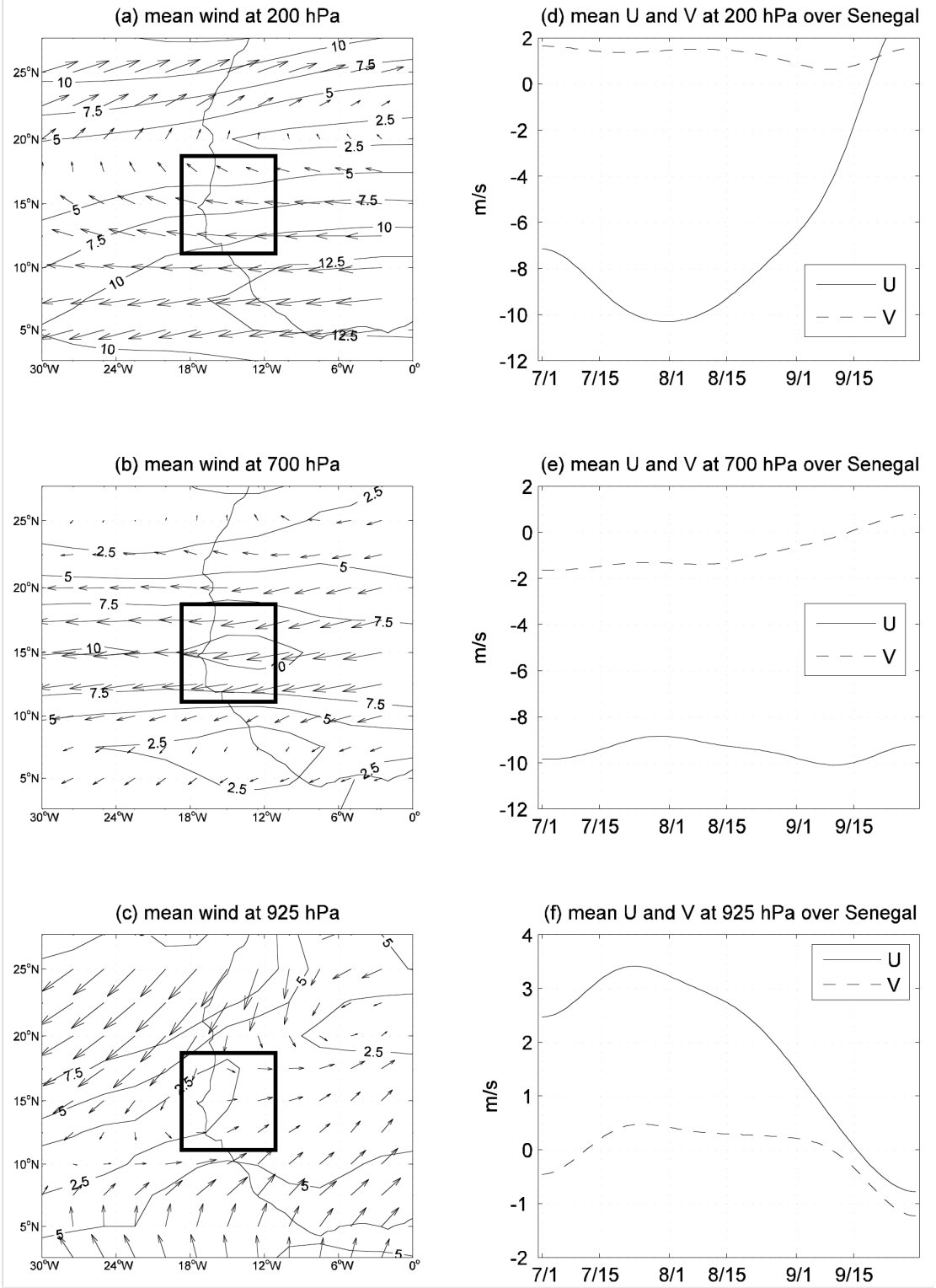
(a) mean wind at 200 hPa
(b) mean wind at 700 hPa
(c) mean wind at 925 hPa
(d) mean U and V at 200 hPa over Senegal
(e) mean U and V at 700 hPa over Senegal
(f) mean U and V at 925 hPa over Senegal
m/s
U
V
7/1
7/15
8/1
8/15
9/1
9/15
30°W
24°W
18°W
12°W
6°W
0°
25°N
20°N
15°N
10°N
5°N

FIG. 2

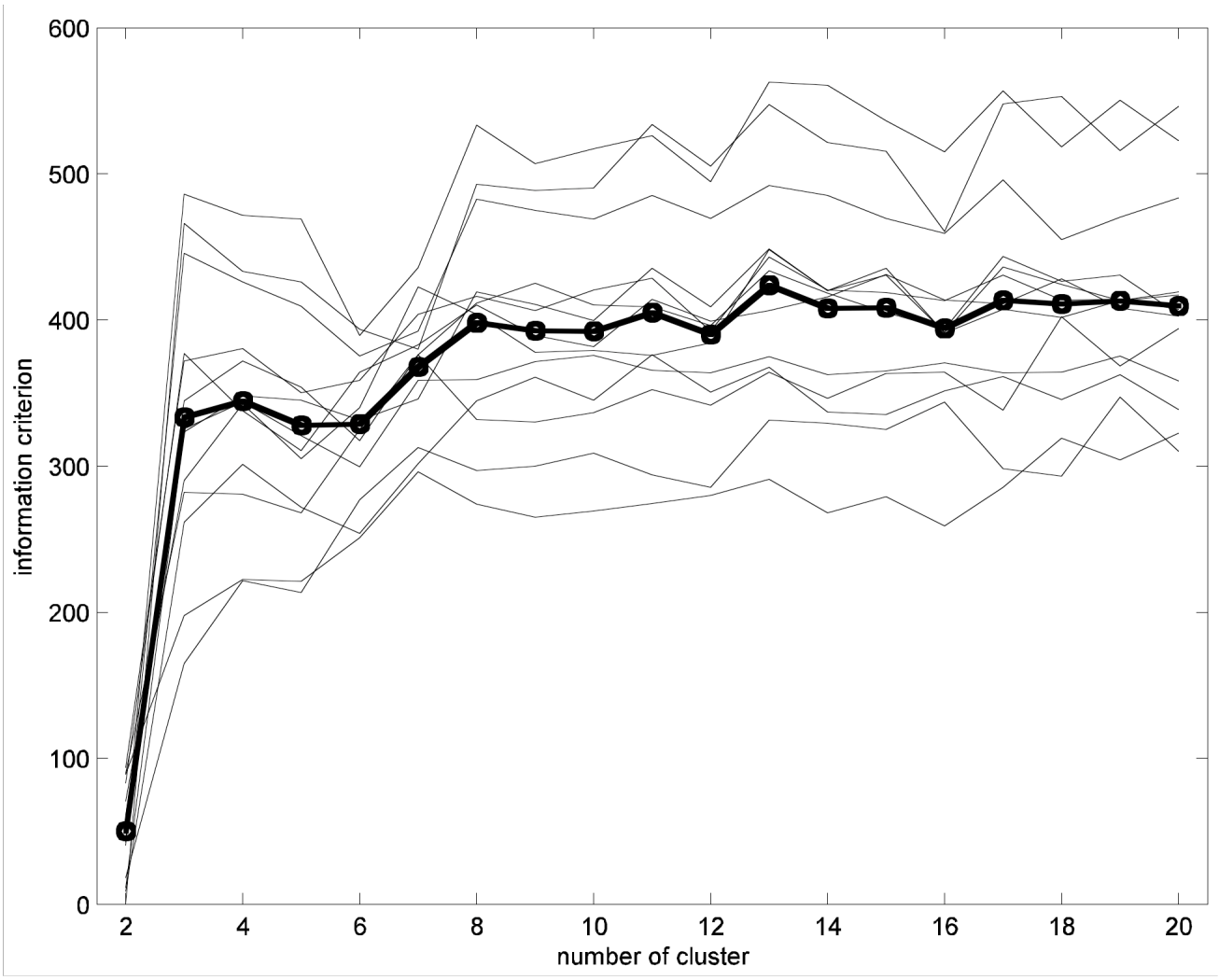
600
500
400
300
200
100
0
information criterion
2
4
6
8
10
12
14
16
18
20
number of cluster
FIG.3

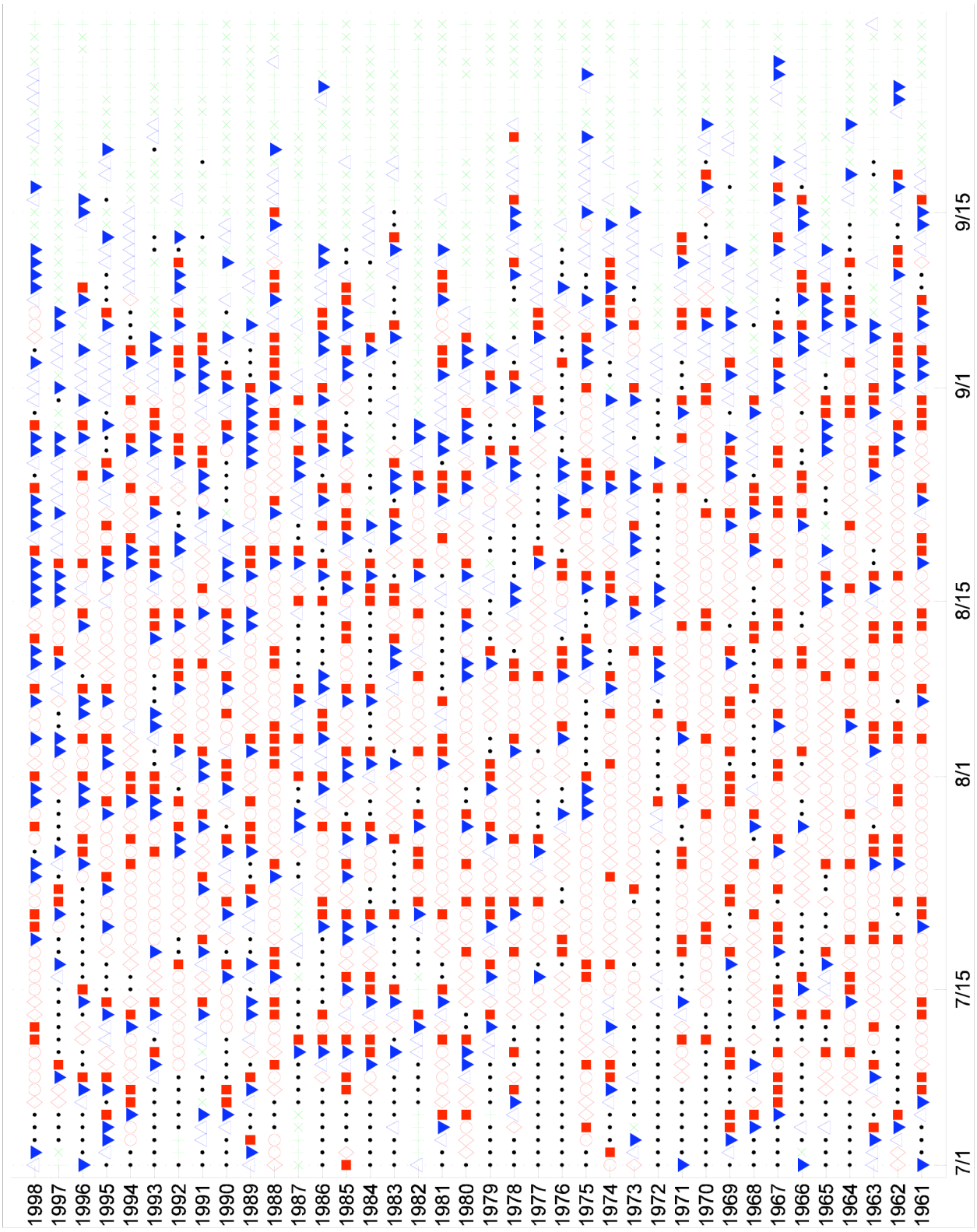
1998
1997
1996
1995
1994
1993
1992
1991
1990
1989
1988
1987
1986
1985
1984
1983
1982
1981
1980
1979
1978
1977
1976
1975
1974
1973
1972
1971
1970
1969
1968
1967
1966
1965
1964
1963
1962
1961
7/1
7/15
8/1
8/15
9/1
9/15

FIG. 4

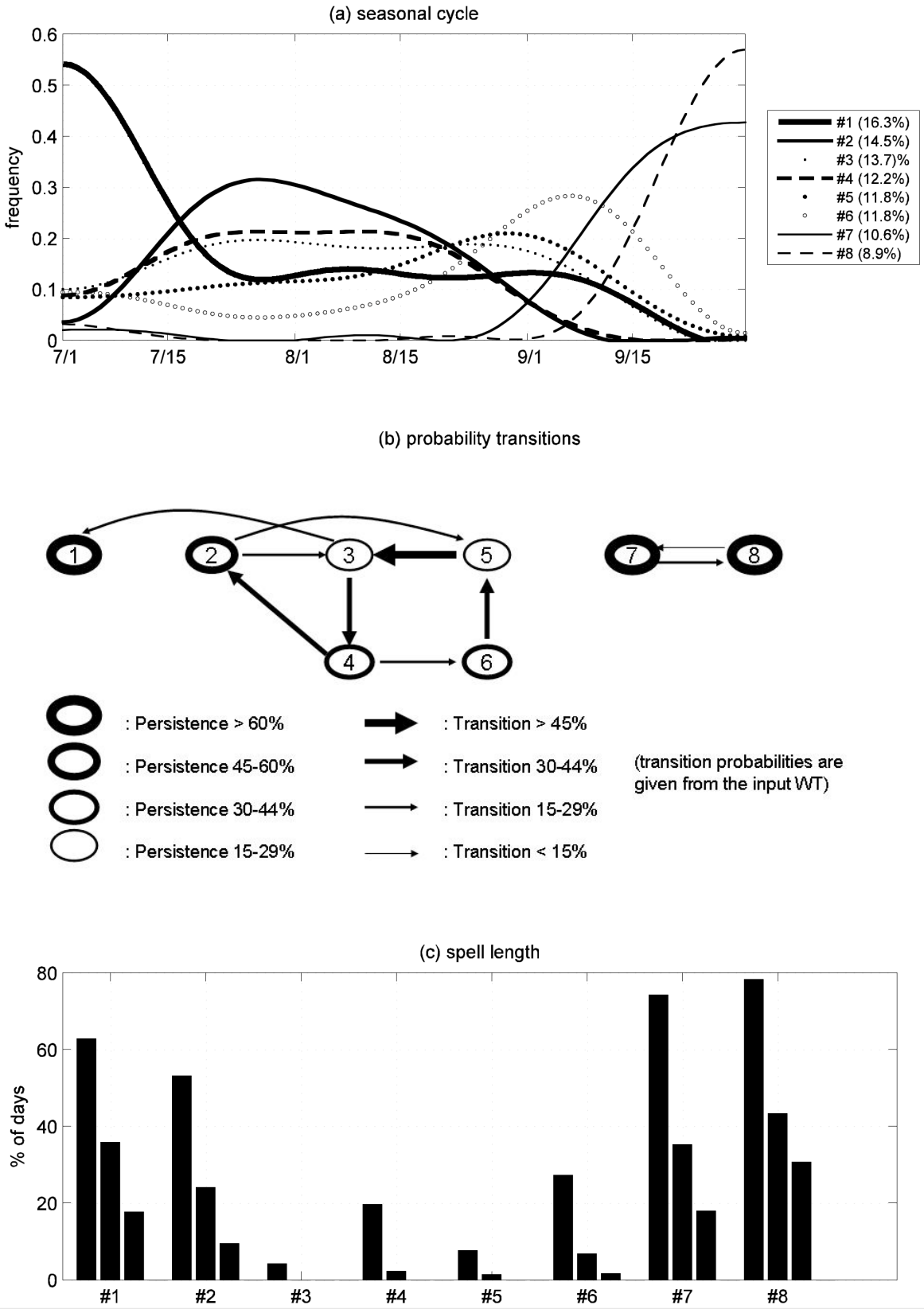
(a) seasonal cycle
frequency
0.6
0.5
0.4
0.3
0.2
0.1
0
7/1
7/15
8/1
8/15
9/1
9/15
#1 (16.3%)
#2 (14.5%)
#3 (13.7)%
#4 (12.2%)
#5 (11.8%)
#6 (11.8%)
#7 (10.6%)
#8 (8.9%)
(b) probability transitions
1
2
3
4
5
6
7
8
: Persistence > 60%
: Persistence 45-60%
: Persistence 30-44%
: Persistence 15-29%
: Transition > 45%
: Transition 30-44%
: Transition 15-29%
: Transition < 15%
(transition probabilities are given from the input WT)
(c) spell length
% of days
80
60
40
20
0
#1
#2
#3
#4
#5
#6
#7
#8

FIG. 5

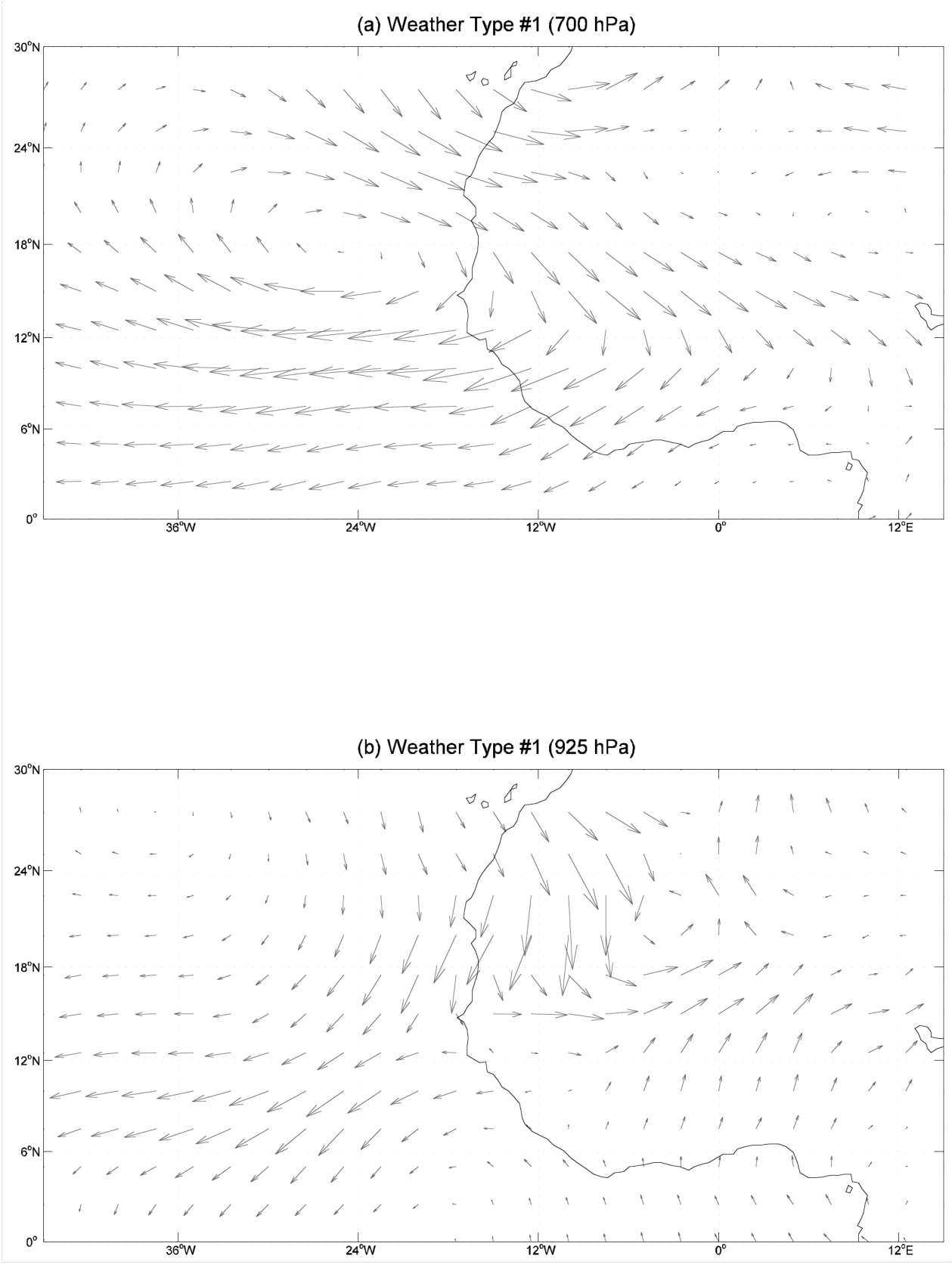
(a) Weather Type #1 (700 hPa)
30°N
24°N
18°N
12°N
6°N
0°
36°W
24°W
12°W
0°
12°E
(b) Weather Type #1 (925 hPa)
30°N
24°N
18°N
12°N
6°N
0°
36°W
24°W
12°W
0°
12°E

FIG. 6

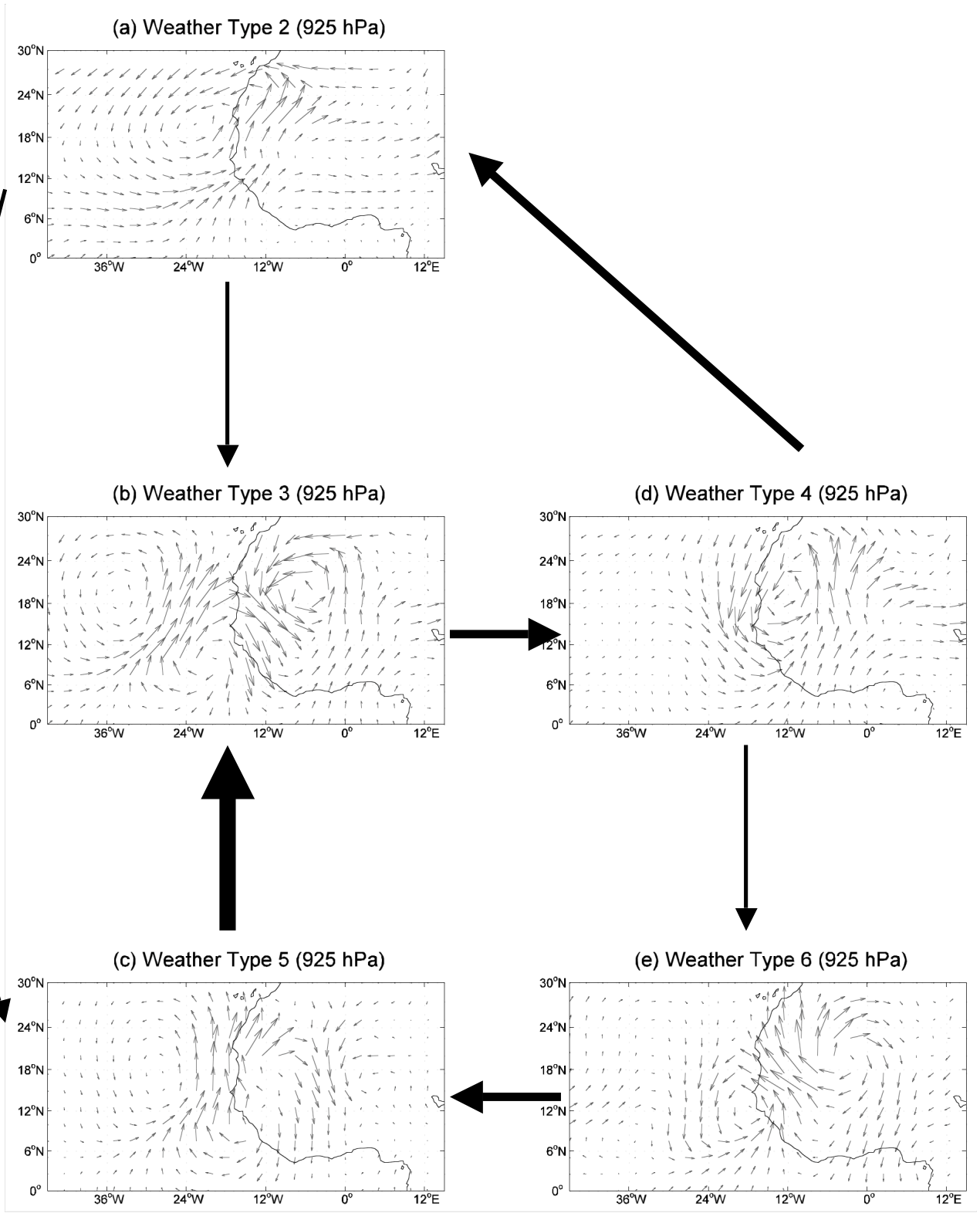
(a) Weather Type 2 (925 hPa)
(b) Weather Type 3 (925 hPa)
(d) Weather Type 4 (925 hPa)
(c) Weather Type 5 (925 hPa)
(e) Weather Type 6 (925 hPa)
30°N
24°N
18°N
12°N
6°N
0°
36°W
24°W
12°W
0°
12°E

FIG. 7

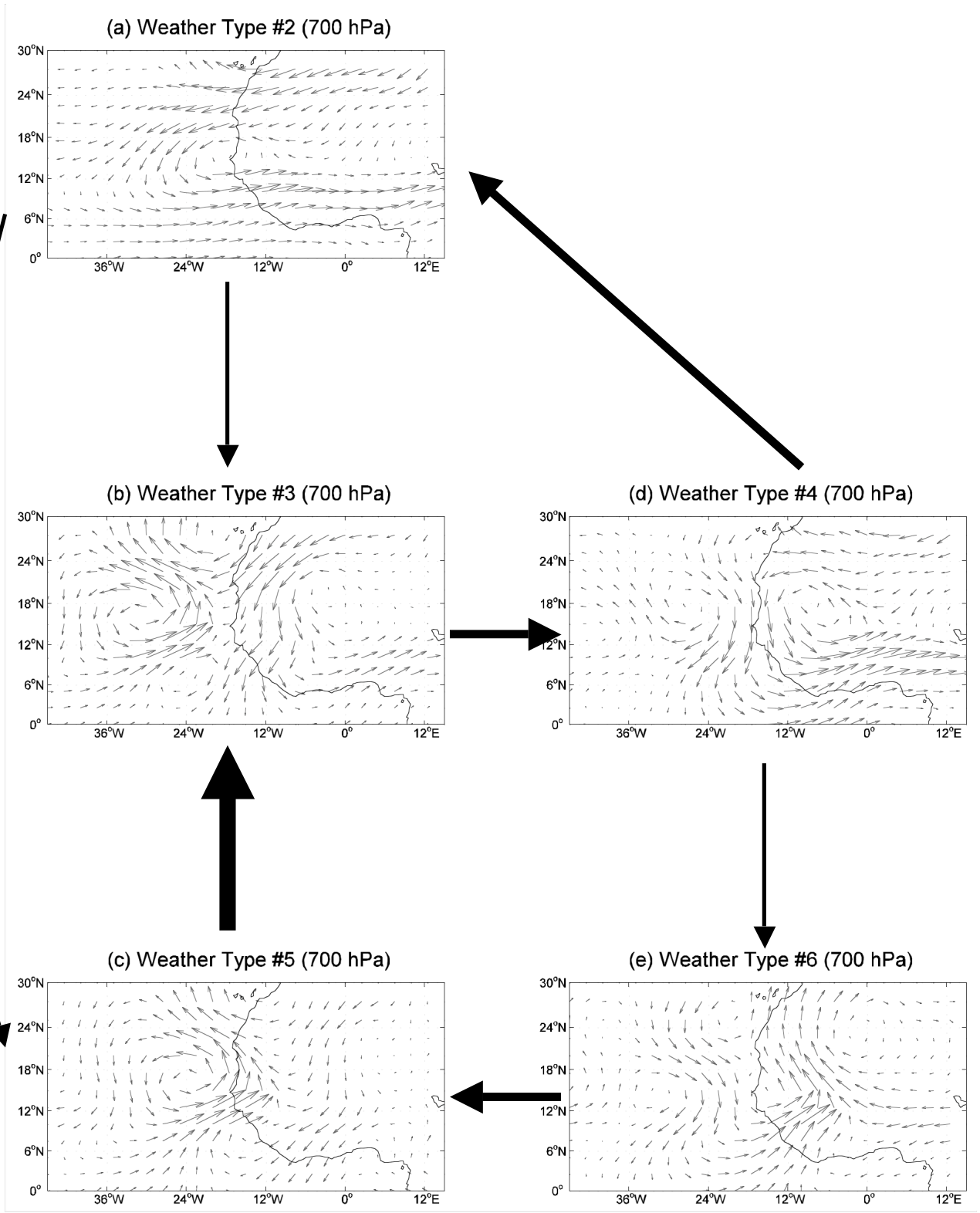
(a) Weather Type #2 (700 hPa)
(b) Weather Type #3 (700 hPa)
(d) Weather Type #4 (700 hPa)
(c) Weather Type #5 (700 hPa)
(e) Weather Type #6 (700 hPa)
30°N
24°N
18°N
12°N
6°N
0°
36°W
24°W
12°W
0°
12°E

FIG. 8

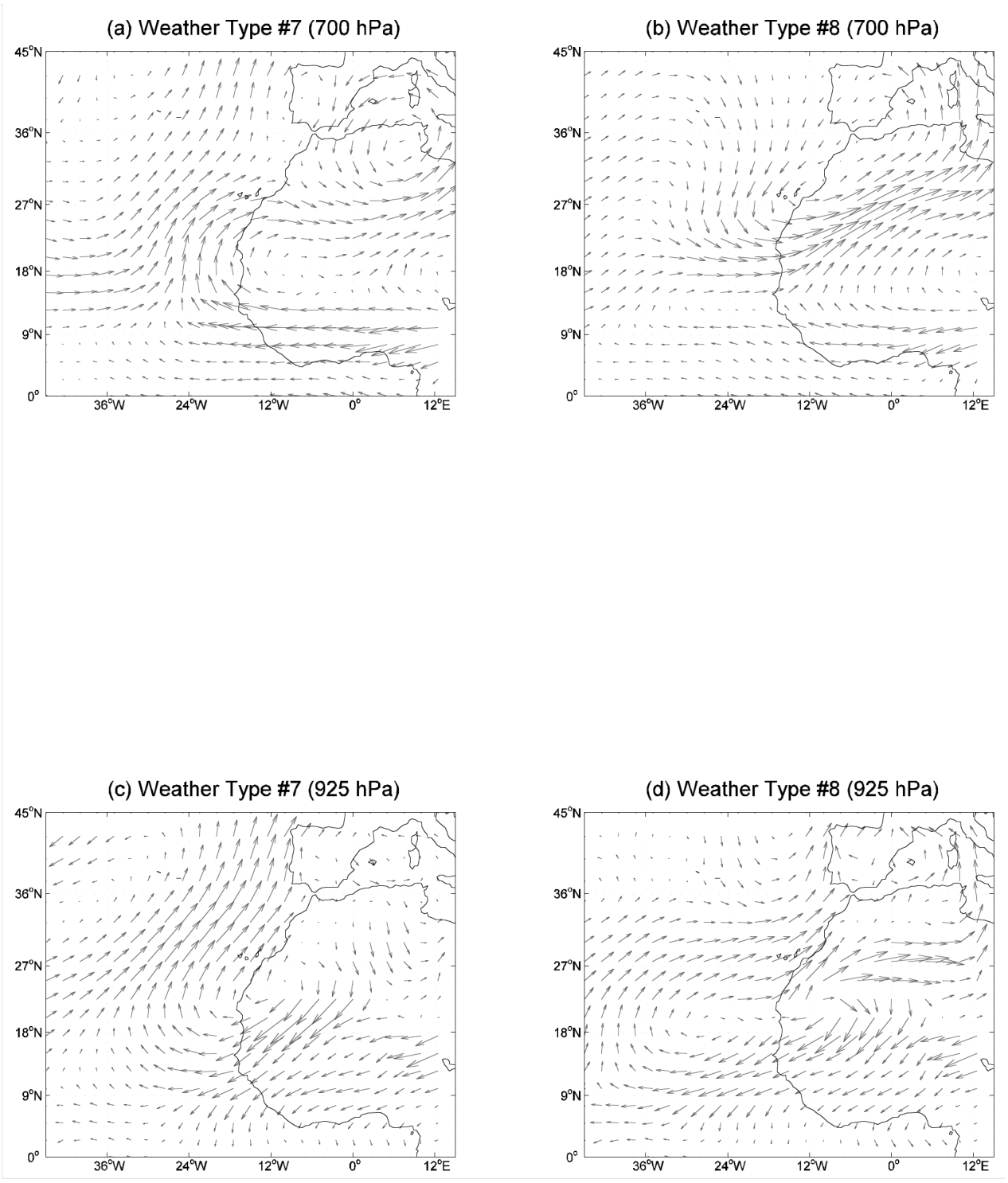
(a) Weather Type #7 (700 hPa)
(b) Weather Type #8 (700 hPa)
(c) Weather Type #7 (925 hPa)
(d) Weather Type #8 (925 hPa)
45°N
36°N
27°N
18°N
9°N
0°
36°W
24°W
12°W
0°
12°E

FIG. 9

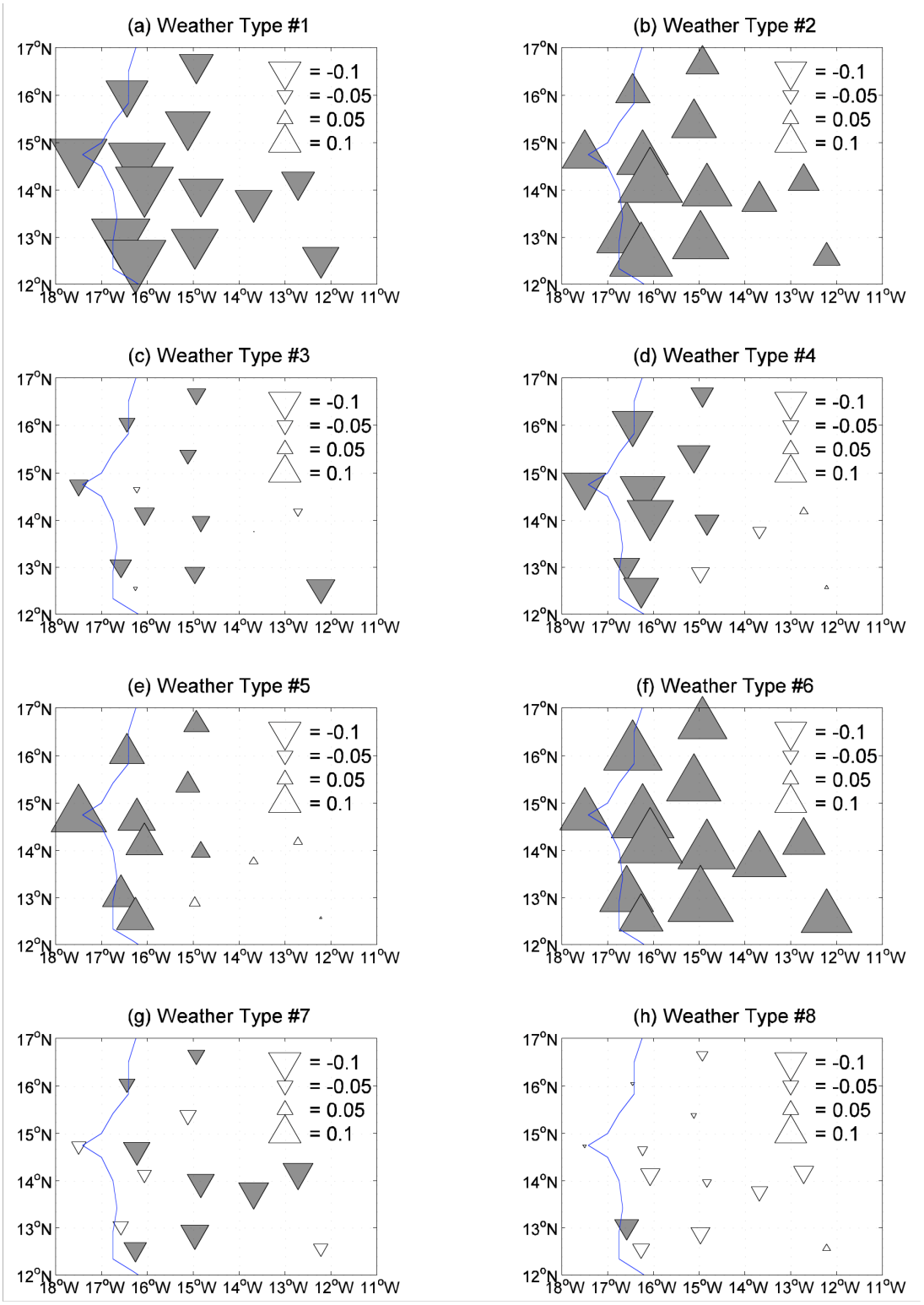
(a) Weather Type #1
(b) Weather Type #2
(c) Weather Type #3
(d) Weather Type #4
(e) Weather Type #5
(f) Weather Type #6
(g) Weather Type #7
(h) Weather Type #8
= -0.1
= -0.05
= 0.05
= 0.1
17°N
16°N
15°N
14°N
13°N
12°N
18°W 17°W 16°W 15°W 14°W 13°W 12°W 11°W

FIG. 10

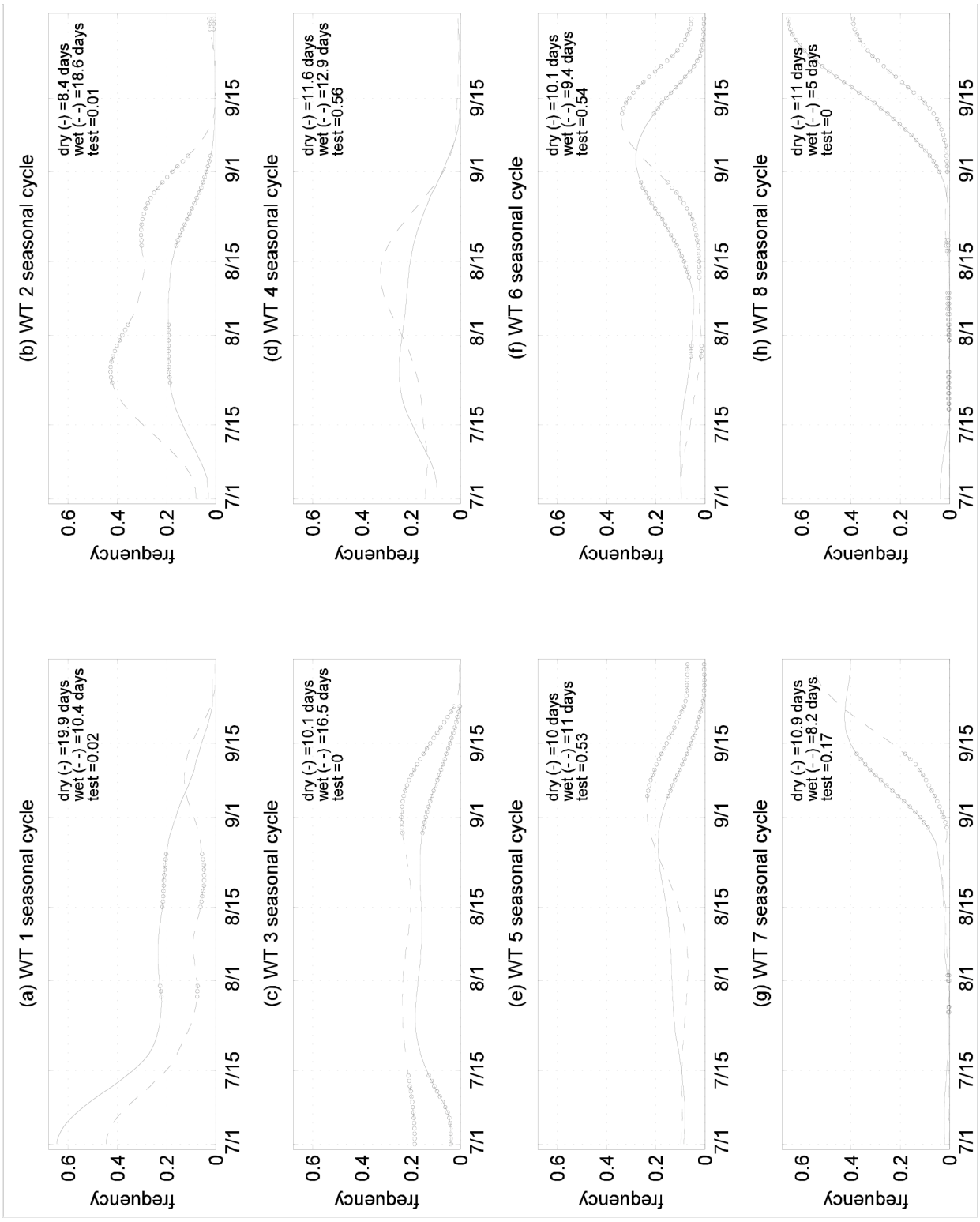
(a) WT 1 seasonal cycle
dry (-) =19.9 days
wet (- -) =10.4 days
test =0.02
(b) WT 2 seasonal cycle
dry (-) =8.4 days
wet (- -) =18.6 days
test =0.01
(c) WT 3 seasonal cycle
dry (-) =10.1 days
wet (- -) =16.5 days
test =0
(d) WT 4 seasonal cycle
dry (-) =11.6 days
wet (- -) =12.9 days
test =0.56
(e) WT 5 seasonal cycle
dry (-) =10 days
wet (- -) =11 days
test =0.53
(f) WT 6 seasonal cycle
dry (-) =10.1 days
wet (- -) =9.4 days
test =0.54
(g) WT 7 seasonal cycle
dry (-) =10.9 days
wet (- -) =8.2 days
test =0.17
(h) WT 8 seasonal cycle
dry (-) =11 days
wet (- -) =5 days
test =0
frequency
0
0.2
0.4
0.6
7/1
7/15
8/1
8/15
9/1
9/15

FIG. 11

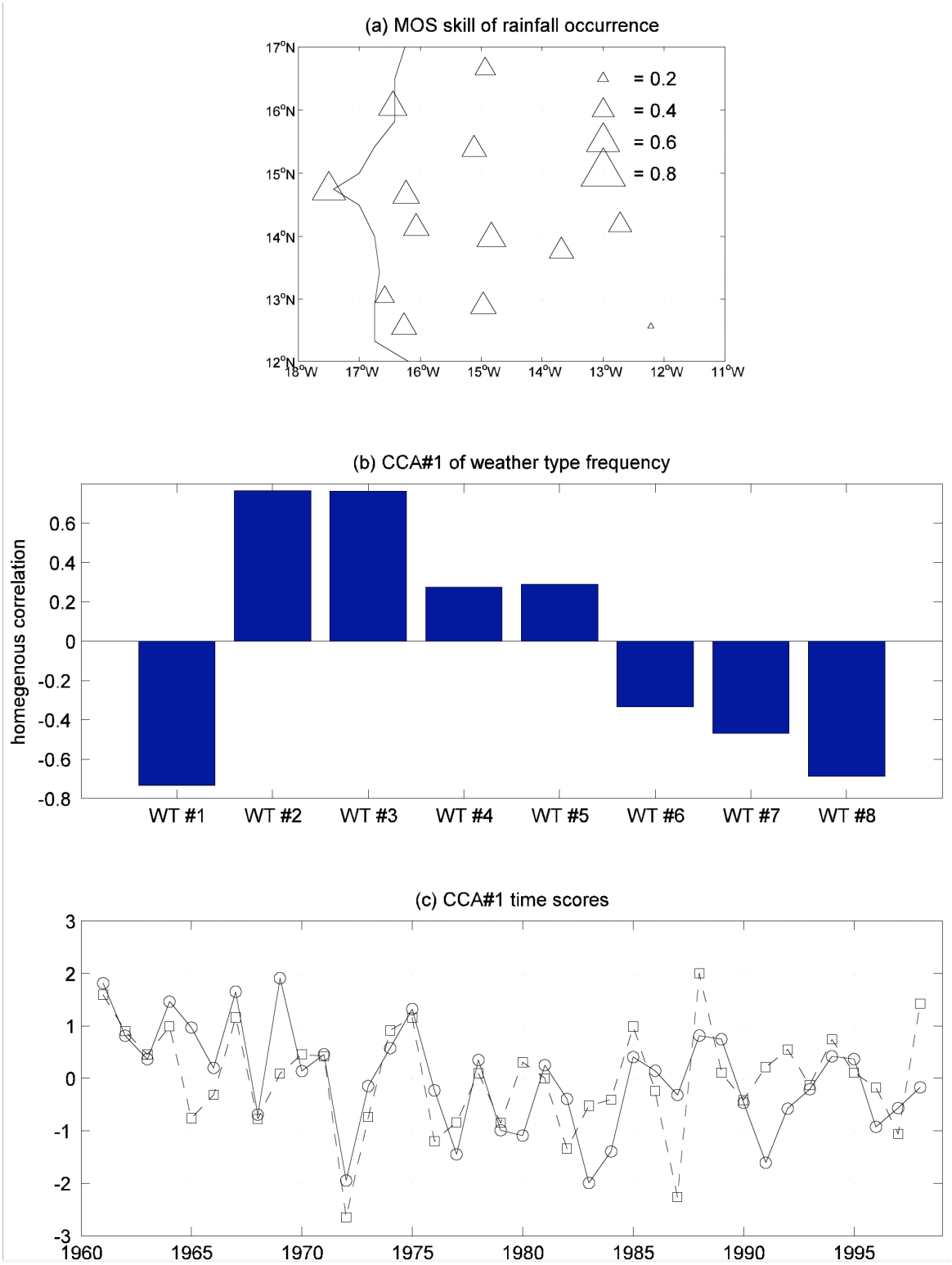
(a) MOS skill of rainfall occurrence
17°N
16°N
15°N
14°N
13°N
12°N
18°W
17°W
16°W
15°W
14°W
13°W
12°W
11°W
= 0.2
= 0.4
= 0.6
= 0.8
(b) CCA#1 of weather type frequency
homegenous correlation
0.6
0.4
0.2
0
-0.2
-0.4
-0.6
-0.8
WT #1
WT #2
WT #3
WT #4
WT #5
WT #6
WT #7
WT #8
(c) CCA#1 time scores
3
2
1
0
-1
-2
-3
1960
1965
1970
1975
1980
1985
1990
1995

FIG. 12

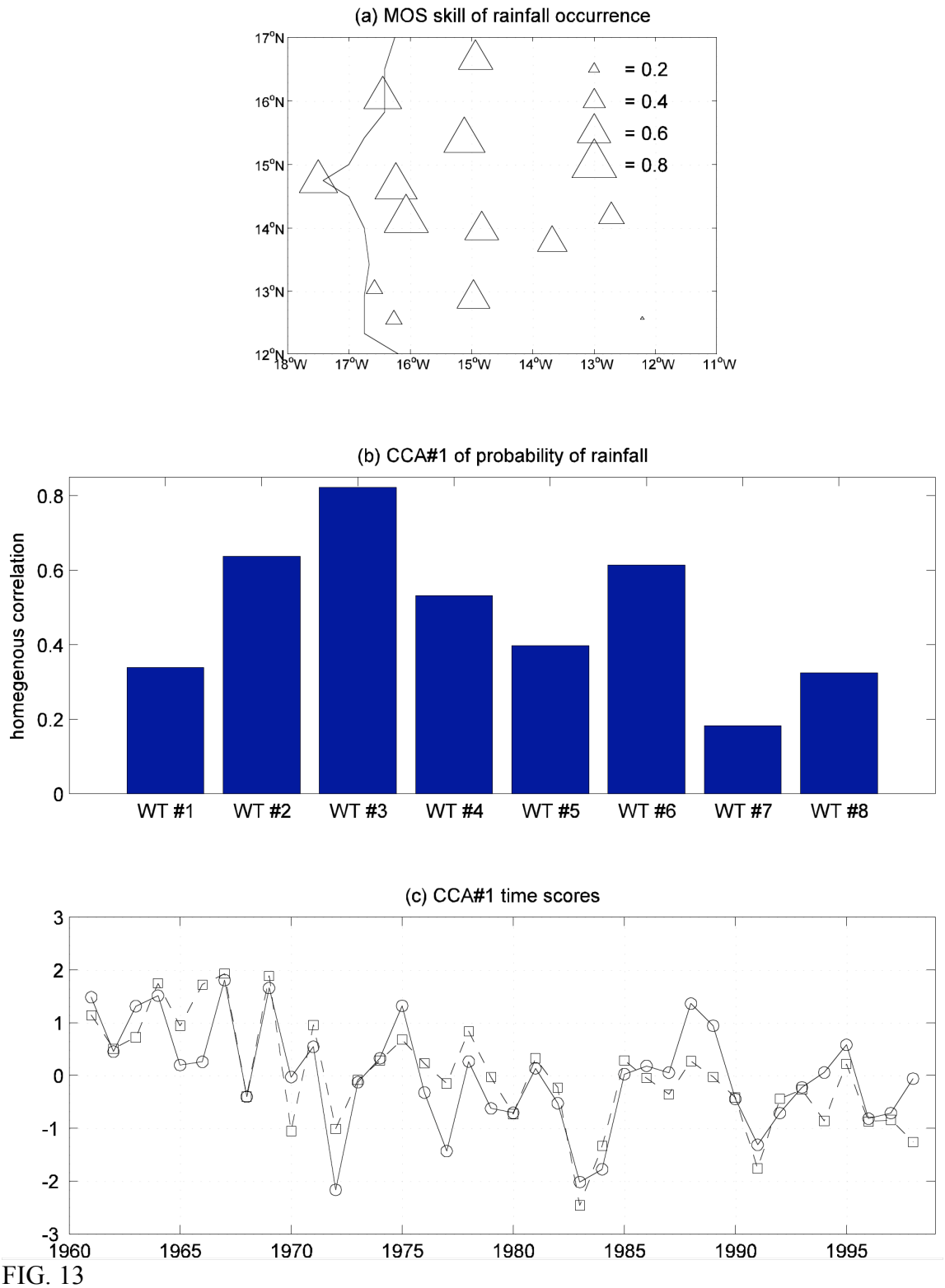
(a) MOS skill of rainfall occurrence
17°N
16°N
15°N
14°N
13°N
12°N
18°W
17°W
16°W
15°W
14°W
13°W
12°W
11°W
= 0.2
= 0.4
= 0.6
= 0.8
(b) CCA#1 of probability of rainfall
homegenous correlation
0
0.2
0.4
0.6
0.8
WT #1
WT #2
WT #3
WT #4
WT #5
WT #6
WT #7
WT #8
(c) CCA#1 time scores
3
2
1
0
-1
-2
-3
1960
1965
1970
1975
1980
1985
1990
1995

FIG. 13

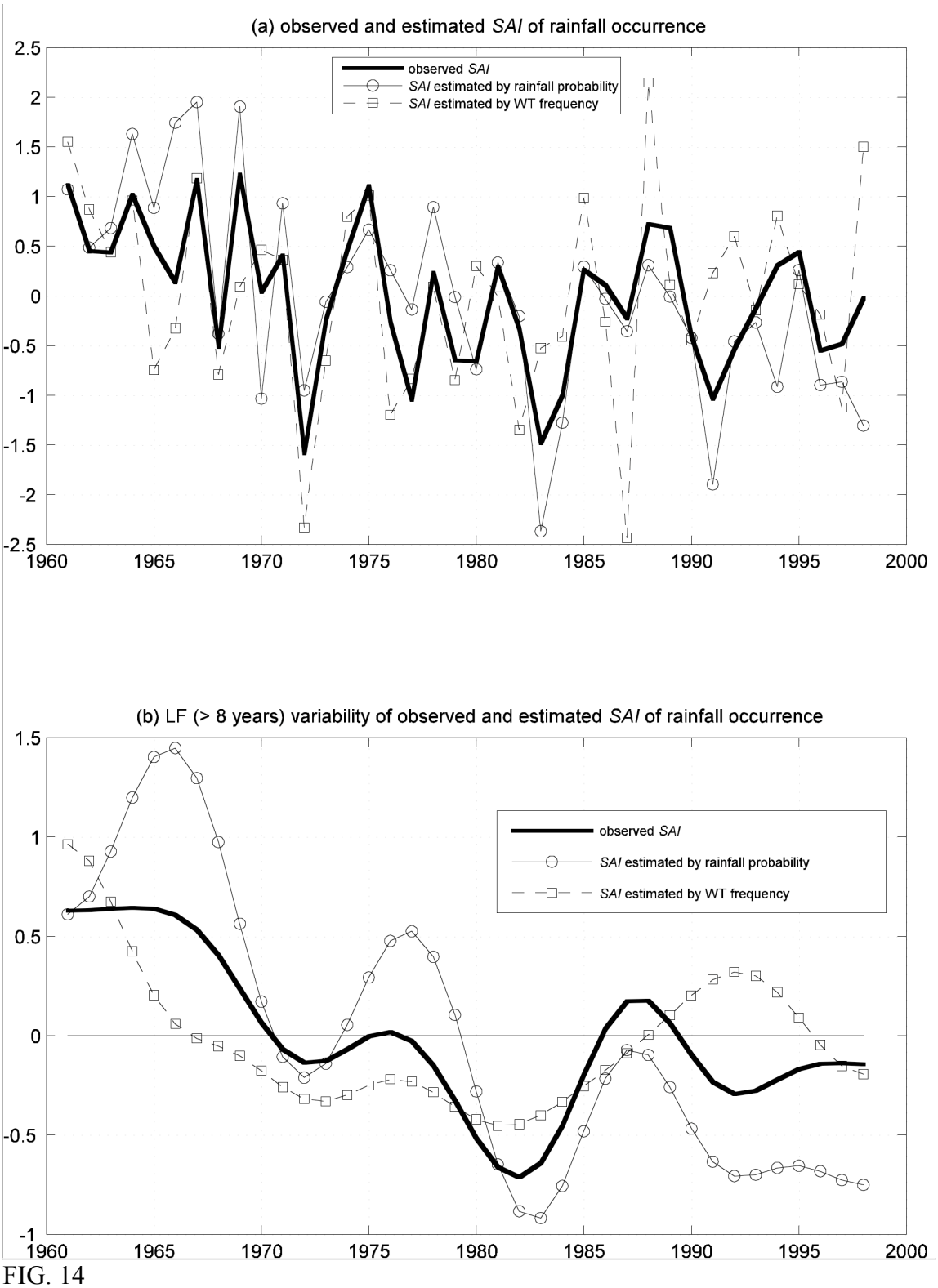
(a) observed and estimated SAI of rainfall occurrence
observed SAI
SAI estimated by rainfall probability
SAI estimated by WT frequency
2.5
2
1.5
1
0.5
0
-0.5
-1
-1.5
-2
-2.5
1960
1965
1970
1975
1980
1985
1990
1995
2000
(b) LF (> 8 years) variability of observed and estimated SAI of rainfall occurrence
observed SAI
SAI estimated by rainfall probability
SAI estimated by WT frequency
1.5
1
0.5
0
-0.5
-1
1960
1965
1970
1975
1980
1985
1990
1995
2000
FIG. 14

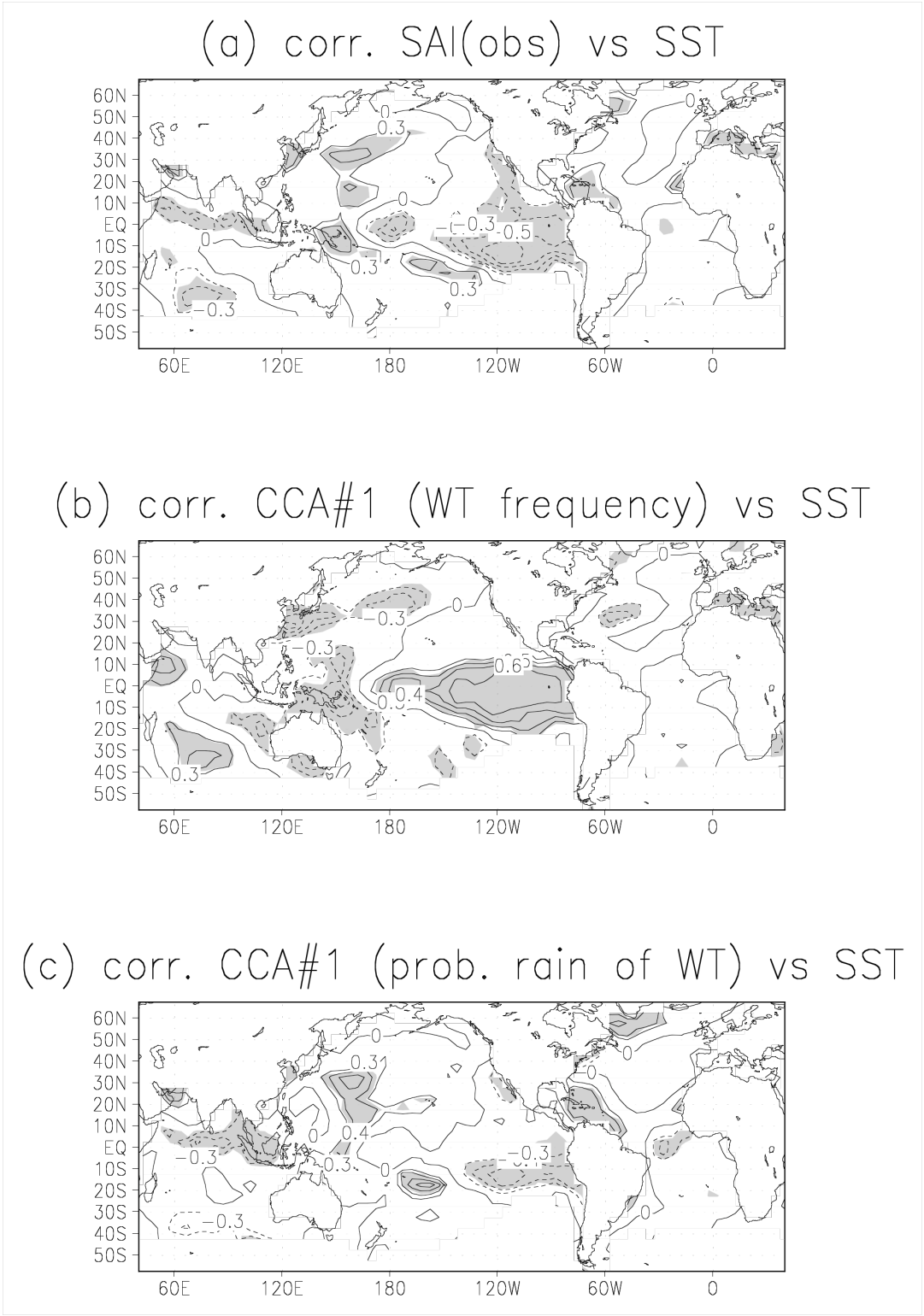
(a) corr. SAI(obs) vs SST
60N
50N
40N
30N
20N
10N
EQ
10S
20S
30S
40S
50S
60E
120E
180
120W
60W
0
0.3
−0.3
0.5
(b) corr. CCA#1 (WT frequency) vs SST
0.6
0.4
(c) corr. CCA#1 (prob. rain of WT) vs SST

FIG. 15